




Global-Scale Processes and Effects of Magnetic Reconnection on the Geospace Environment

S.A. Fuselier^{1,2}  · S.M. Petrinec³ · P.H. Reiff⁴ · J. Birn⁵ · D.N. Baker⁶ · I.J. Cohen⁷ · R. Nakamura⁸ · M.I. Sitnov⁷ · G.K. Stephens⁷ · J. Hwang¹ · B. Lavraud⁹ · T.E. Moore¹⁰ · K.J. Trattner⁶ · B.L. Giles¹⁰ · D.J. Gershman¹⁰ · S. Toledo-Redondo¹¹ · J.P. Eastwood¹²

Received: 17 May 2023 / Accepted: 8 April 2024
© The Author(s) 2024

Abstract

Recent multi-point measurements, in particular from the Magnetospheric Multiscale (MMS) spacecraft, have advanced the understanding of micro-scale aspects of magnetic reconnection. In addition, the MMS mission, as part of the Heliospheric System Observatory, combined with recent advances in global magnetospheric modeling, have furthered the understanding of meso- and global-scale structure and consequences of reconnection. Magnetic reconnection at the dayside magnetopause and in the magnetotail are the drivers of the global Dungey cycle, a classical picture of global magnetospheric circulation. Some recent advances in the global structure and consequences of reconnection that are addressed here include a detailed understanding of the location and steadiness of reconnection at the dayside magnetopause, the importance of multiple plasma sources in the global circulation, and reconnection consequences in the magnetotail. These advances notwithstanding, there are important questions about global reconnection that remain. These questions focus on how multiple reconnection and reconnection variability fit into and complicate the Dungey Cycle picture of global magnetospheric circulation.

Keywords Magnetic reconnection · Global magnetospheric circulation · Magnetopause · Magnetospheric cusps · Magnetotail

1 Magnetic Reconnection and the Dungey Cycle

In the absence of magnetic reconnection at the magnetopause, magnetic field lines in the magnetosheath and magnetosphere have no interconnection. Magnetosheath field lines ultimately trace back to the Sun and are considered “solar wind” field lines, with no connection with the Earth’s ionosphere. Field lines in the low-latitude magnetosphere trace back to the high-latitude ionosphere in both northern and southern hemispheres and are considered “closed”. When the interplanetary magnetic field (IMF) is southward, magnetic reconnection at the magnetopause occurs at relatively low latitudes between these magnetosheath and magnetospheric magnetic field lines. Reconnection at the low-latitude magnetopause “opens” previously closed magnetospheric field lines so that they trace back to the high-latitude ionosphere in one direction along the magnetic field and ultimately to interplanetary

Extended author information available on the last page of the article

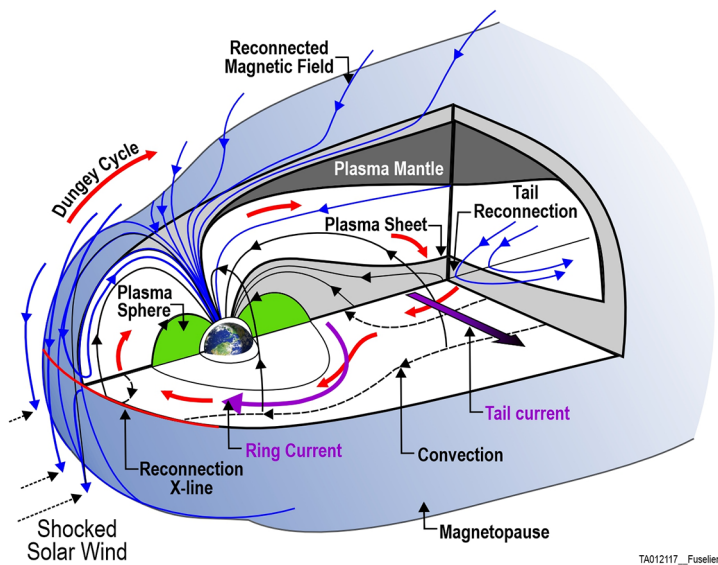


Fig. 1 3-D schematic of the Dungey cycle. For southward IMF and no dipole tilt, reconnection occurs along a long line across the dayside magnetopause. Reconnected field lines convect over the pole and into the magnetotail. Reconnection in the magnetotail closes the previously open field lines. Convection brings these closed field lines from the tail back to the dayside to complete the cycle. This cycle is depicted by the red arrows

space in the opposite direction. This opening of previously closed field lines was depicted schematically for the magnetosphere for the first time by Dungey (1961).

Under the convection of the solar wind, these reconnected field lines are dragged over the poles towards the Earth's magnetotail. Magnetic reconnection in the magnetotail re-connects the previously open field lines, forming newly re-closed field lines. Through the action of magnetospheric convection, these closed field lines convect earthward and finally return to the dayside. A two-dimensional version of this model for an open magnetosphere was first published by Dungey (1962) in a free-hand sketch. However, the model in fact dates back to Dungey's PhD thesis (Dungey 1950). A fascinating and detailed account of the realization that reconnection plays a critical role in magnetospheric dynamics (which was considered quite radical at the dawn of the space age) is found in: *Magnetospheric plasma physics: The impact of Jim Dungey's research* (2015).

A quasi-three-dimensional schematic depiction of this plasma and field circulation is shown in Fig. 1. With an IMF pointing due southward and no dipole tilt, magnetic field lines in the Earth's magnetosheath reconnect along a long reconnection X-line oriented across the dayside magnetopause through the subsolar region. These reconnected field lines (in blue) are dragged over the poles into the magnetotail. In the magnetotail, the field lines (in black) reconnect and snap sunward. Eventually, they convect around the Earth (a black field line shown in Fig. 1 is convecting sunward and duskward) and return to the subsolar region. The circulation is shown by the red arrows.

In the original model of a magnetosphere driven by reconnection at the magnetopause and in the magnetotail, the reconnection rates at the dayside and in the tail are the same. An important complication in this reconnection-driven circulation model is that the dayside and nightside rates are almost always different. Typically, dayside reconnection occurs continuously (e.g., Russell 1972) with possible variable rate while nightside reconnection

is very intermittent (e.g., Russell 1972), especially in the near-Earth magnetotail ~ 20 – 30 Earth Radii (R_E) from the Earth. The dayside rate is reflected in the polar cap potential and changes in the dayside and nightside rates are reflected in the size of the polar cap inside the auroral oval.

A revision of the Dungey circulation model that describes the magnetospheric substorm process was introduced by Hones (1977). In this revision, magnetic flux transferred from the dayside builds up in the magnetotail during an interval when there is dayside reconnection and no reconnection in the near-Earth magnetotail. This flux buildup causes the tail to stretch until explosive reconnection in the near-tail re-connects the field lines. During this explosive reconnection, the reconnection rate in the near-tail may exceed that on the dayside. Averaging over a long time, the flux transfer rate from the dayside must match the nightside rate. However, at any given instant in time they can differ: if the dayside rate is larger, the polar cap expands; if the nightside rate is larger, the polar cap shrinks (Cowley and Lockwood 1992). This model is often referred to as the Expanding-Contracting Polar Cap Model (see e.g., Milan et al. 2017)

In this paper, the global-scale processes and effects of magnetic reconnection are reviewed in the context of this revised Dungey circulation model. For Sects. 2–5, the focus is on southward IMF conditions. Section 2 describes global magnetic reconnection at the dayside magnetopause and the initiation of the Dungey cycle. Section 3 describes field line convection from the dayside to the nightside and implications for the Earth's magnetospheric cusps and the polar cap potential. Section 4 describes reconnection in the Earth's magnetotail. Section 5 describes convection of reconnected field lines back to the dayside and the completion of the Dungey cycle. Section 6 describes the changes to the Dungey cycle when the IMF is northward or when the IMF has a dominant B_X component, i.e., when the IMF is nearly radial. Finally, Sect. 7 describes the complications to the Dungey cycle when magnetic reconnection at the dayside is variable in space and/or in time and when nightside reconnection has time and potentially spatial variability outside of the large-scale variability that occurs in the substorm process.

2 Global Magnetic Reconnection at the Dayside Magnetopause

2.1 Evidence for Long “Primary” Reconnection X-Lines

Observations of charged particles within the magnetospheric cusps provide remote sensing evidence for the presence of collisionless magnetic reconnection at the magnetopause. For a cusp-crossing satellite that observes precipitating magnetosheath ions during southward IMF, the extent of the reconnection X-lines is estimated by tracing magnetic field lines from the cusp to the dayside magnetopause. Ion precipitation observations over a range of local times during such a cusp traversal are exploited to determine the large-scale configuration (orientation(s)) of the primary reconnection X-line(s) along the magnetopause. This method yields primary X-lines that are continuous over many R_E (e.g., Trattner et al. (2005), Trattner et al. (2007)). The method was applied to 130 cusp traversals and, because these cusp traversals cover a finite and rather large range of geomagnetic latitudes, these observations provide one of the better estimates of the length of the primary X-line. Continuous X-line lengths of many R_E were observed, with the measured length limited only by the magnetic local time coverage of the cusp traversal. The term “primary” is used here to indicate a long, quasi-stable X-line as opposed to a transient X-line or lines that might be produced in a Flux Transfer Event (FTE) (Fuselier et al. 2019b) (see also Sect. 7).

Another remote sensing method for estimating the reconnection X-line extent is to utilize space-based global auroral imagers (e.g., Fuselier et al. 2002). Doppler-shifted proton auroral emissions result from the precipitation of energetic (> 2 keV) protons into the ionosphere. These protons are accelerated in the reconnection process at the magnetopause. Therefore, the precipitation pattern in the ionosphere of these energetic protons provides the foot-points of reconnected magnetic field lines. These foot-points are mapped to the magnetopause using a closed form of the magnetospheric magnetic field to determine the “last closed field line”, i.e., the field line that undergoes reconnection to produce the proton precipitation. This mapping method also shows that reconnection X-lines during southward IMF extend over a wide span of local times along the dayside magnetopause, with equivalent extents of $\sim 10 - 25 R_E$ (Fuselier et al. 2002, 2003; Berchem et al. 2003; Phan et al. 2006; Dunlop et al. 2011). Although this method for estimating the X-line extent has been done for only a few events, these results are in good agreement with the results from the much larger number of cusp traversals discussed above.

For in situ observations at the magnetopause, single-point in situ observations of the presence of magnetopause magnetic reconnection are rather common (typically by observing accelerated ion flows tangent to the magnetopause). However, in situ evidence for long, quasi-continuous reconnection lines is quite rare, because simultaneous in situ observations are required from multiple locations and it is not clear if the reconnection line is continuous between the spacecraft. Such events typically involve multiple, widely spaced spacecraft sampling the magnetopause at approximately the same time during an interval of steady IMF with a southward-directed component, with each observing reconnection signatures (e.g., Peterson et al. 1998; Phan et al. 2000; Dunlop et al. 2011; Toledo-Redondo et al. 2021b). If the spacecraft happen to be positioned such that different spacecraft observe accelerated ion flows in opposing directions (e.g., Phan et al. 2000), then this provides additional information that the extended reconnection line is situated somewhere between the spacecraft. This multi-spacecraft technique for estimating the reconnection X-line length was extended to a number of magnetopause conjunctions by the THEMIS spacecraft (Walsh et al. 2017; Zou et al. 2019, 2020; Atz et al. 2022). While some of the THEMIS conjunctions are consistent with long X-lines, many are not. The discrepancy between these results and all of the other results discussed above may be the use of the Walen test, a very restrictive definition of reconnection at the magnetopause that was employed in the THEMIS conjunctions. The Walen test is a single fluid test that determines if the magnetopause is consistent with an infinite, one-dimensional rotational discontinuity. It fails to take into account the multi-component nature of the plasma, the flow in the magnetosheath, and multiple reconnection at the magnetopause, which is quite common (see, e.g., Vines et al. 2017, and Sect. 7). In essence, this test is sufficient for identifying reconnection at the magnetopause, but it is far from necessary.

2.2 The Maximum Magnetic Shear Model and Long, Continuous Reconnection X-Lines

As described in the previous section, magnetic reconnection readily occurs along extended X-lines over the dayside magnetopause when the IMF is southward, extending from local noon far along the magnetopause flanks. This results in the transport of solar wind flux into the magnetosphere and erosion of the dayside magnetosphere. The location, extent, and configuration of the extended reconnection line along the dayside magnetopause have been the subject of many studies during the past few decades. Some early models predicted long reconnection lines would occur exclusively along anti-parallel merging regions along

the magnetopause; extending from low latitudes at the flanks up to the cusp region near local noon (Crooker 1979; Luhmann et al. 1984). Other parameters and models that consider various aspects of collisionless reconnection and include segments of anti-parallel and component reconnection are: a uniform guide field or B_M component (Sonnerup 1974; Gonzalez and Mozer 1974), the angle of bisection between magnetic fields earthward/sunward of the magnetopause (Moore et al. 2002, 2008; Borovsky 2008; Hesse et al. 2013), maxima of the asymmetric reconnection outflow speed (Swisdak and Drake 2007), maxima of the asymmetric Sweet-Parker reconnection rate (Borovsky 2013), maxima of the current density magnitude (Alexeev et al. 1998), and the Maximum Magnetic Shear model (Trattner et al. 2007).

The Maximum Magnetic Shear Model, described in much greater detail in Trattner et al. (2021a), was developed from numerous observations of ion distribution functions and velocity cutoffs within the mid- to high-altitude northern cusp region, systematically traced from the observing spacecraft along magnetic field lines to the magnetopause using a time-of-flight methodology to estimate the locations of magnetopause reconnection sites. The aggregate set of such estimates under varying solar wind conditions and season (dipole tilt angle) then led to the development of this empirical model. Although this is an empirical model, it uses models for the draped magnetosheath magnetic field, the magnetopause boundary, and the internal magnetospheric magnetic field. The magnetosheath and magnetospheric magnetic fields in the models do not interact as would occur, for example, in an MHD simulation. Rather, the magnetosheath and magnetospheric models are used in closed form to determine the shear at the magnetopause boundary (Petrinec and Fuselier 2003; Trattner et al. 2007; Trattner et al. 2021a,b). An example magnetic shear angle color contour plot (2-D projection and 3-D coverage over the magnetopause), along with an extended reconnection line is shown in Fig. 2. This model has been tested extensively (see Trattner et al. 2021a,b).

For the MMS mission, the model was used to predict the number of magnetopause crossings near the reconnection X-line at the dayside magnetopause (Griffiths et al. 2011; Fuselier et al. 2016). After the first year of operations, there were several successful tests conducted to determine the efficacy of these predictions (e.g., Petrinec et al. 2016; Fuselier et al. 2017; Trattner et al. 2017). In particular, Trattner et al. (2017) surveyed the first year of MMS operations and identified 302 instances when the spacecraft were near the X-line and then compared these locations with the predicted location of the X-line from the Maximum Magnetic Shear model. The Maximum Magnetic Shear model, with its long X-lines, was accurate $\sim 85\%$ of the time. For more details on the empirical model and the tests, see the recent review article on the location of the magnetopause X-line (Trattner et al. 2021a).

2.3 IMF Clock Angle and Cone Angle Determine the Location of the Reconnection X-Line

As inferred from an examination of a large set of Polar/TIMAS cusp crossings and low-velocity cutoff mappings to the magnetopause reconnection site using plasma distributions, the location of the extended magnetopause reconnection line at a given date and time (i.e., season and dipole tilt angle) is simply controlled by the IMF clock and cone angles. These IMF parameters dictate how the large-scale magnetic shear angle varies over the entire magnetopause surface. As described in the previous section, regions with the largest magnetic shear angles provide the location where the extended, primary reconnection line is established in the empirical maximum magnetic shear model. This observations-based model had been used to examine multiple MMS orbit scenarios during the mission development phase

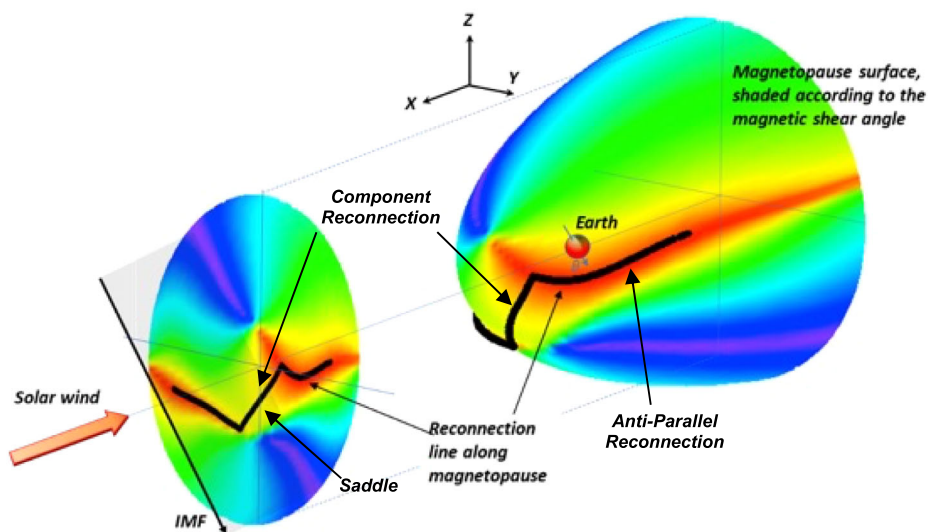


Fig. 2 2-D projection along the Sun-Earth line of the magnetopause surface, and 3-D coverage over the magnetopause, colored according to the magnetic shear angle. A maximum magnetic shear model reconnection X-line across the dayside magnetopause is shown in black. The reconnection line extends from the noon meridian to well along the flanks of the magnetopause

to optimize the likelihood of encountering and directly sampling dayside magnetopause reconnection sites; especially the high-resolution multipoint sampling of the microphysics within the very localized electron diffusion region (Griffiths et al. 2011). This examination proved very beneficial for the prime mission of MMS (Fuselier et al. 2017; Webster et al. 2018). Predicted extended reconnection line locations have subsequently been compared to the MMS observed accelerated ion flow directions. The wide-ranging consistency between the model and observations have provided substantial validation to the conjecture that the location and orientation of the extended reconnection line is controlled primarily by the IMF clock and cone angles at Earth's magnetopause (Petrinec et al. 2016; Trattner et al. 2017), given the boundary condition of the Earth's dipole tilt (Eggington et al. 2020). These single IMF conditions remain true independent of the level of turbulence in the magnetosheath (Petrinec et al. 2022). Obviously, when the clock angle or cone angle rotate, the predicted location of the X-line changes. If the rotation is slow, then the predicted location changes in a way consistent with the Maximum Magnetic Shear model. However, if the rotation is fast, then there is a lag of several minutes as the magnetopause responds to the new IMF orientation (see Trattner et al. 2016)

2.4 Diamagnetic Non-suppression at Earth's Magnetopause

The presence of a pressure gradient (either particle number density or thermal speed) normal to a magnetic field leads to diamagnetic drift. At the magnetopause with magnetic shear across the current layer, an electron pressure gradient normal to a guide field (non-zero component that does not change across the magnetopause) results in an electron diamagnetic drift velocity that is both normal to the guide field and tangent to the magnetopause surface. If component reconnection occurs at the magnetopause along a line representing the guide field, then the diamagnetic drift velocity is along the outflow direction (Cassak and

Fuselier 2016). However, diamagnetic drift may suppress both the onset of reconnection (linear phase) associated with the tearing instability (Coppi et al. 1979; Galeev and Sudan 1984; Zakharov et al. 1993; Rogers and Zakharov 1995), and nonlinear reconnection (Swisdak et al. 2003). Theoretical modeling of this process with the inclusion of some simplifying assumptions leads to a straightforward relation between the jump in the plasma beta across the current layer and the local magnetic shear angle. This relation defines broad regions in parameter space {clock angle (θ), and change in plasma beta across the layer, ($\Delta\beta$) where magnetic reconnection is either 'suppressed' or 'possible'}. For the typical range in the change in plasma beta across the terrestrial magnetopause, reconnection is 'possible' over a large range of magnetic shear angles (Cassak and Fuselier 2016). The lack of diamagnetic suppression for the typical range of plasma conditions is the fundamental reason why the location of reconnection at the Earth's magnetopause is determined by IMF clock and cone angles. There are solar wind conditions for which diamagnetic suppression is expected for parts of the magnetopause surface; however, these conditions are rare in the solar wind at 1 AU and reconnection is typically not suppressed for most of the magnetopause surface the majority of the time.

2.5 Stationarity of Extended Reconnection X-Lines at the Magnetopause

For long intervals of southward IMF, the primary extended reconnection line(s) are also found to be persistent (quasi-stationary) at low- to mid-latitudes (e.g., Frey et al. 2003; Trattner et al. 2021b), extending far along the magnetopause flanks. One example of this behavior was demonstrated with MMS observations by Gomez et al. (2016). During this time, MMS was situated along the dusk flank magnetopause at low latitude and very close to the predicted anti-parallel merging region. Observations of reconnection ion jet reversals tangent to the magnetopause and reversals in heated, streaming electrons switching from parallel to anti-parallel and anti-parallel to parallel to the magnetic field were indicative of a reconnection site passing back and forth over the MMS location. These observations occurred multiple times over a period of ~ 15 minutes, and small changes in the location of the antiparallel reconnection line coincided with small and slow changes in the IMF clock angle. Surprisingly, the X-line passed back and forth over the MMS location even though the ambient bulk tailward flow in the magnetosheath was approximately equal to the Alfvén speed.

The persistence of a quasi-stationary primary reconnection line from two separate magnetopause encounters during intervals of steady IMF clock angle was also noted in a study by Fuselier et al. (2019b). Ion distribution functions observed near the subsolar magnetopause in these separate encounters showed two magnetosheath ion populations, one entering the magnetosphere and one returning from the ionosphere. These two populations were used to remotely locate and track the reconnection line in the same way that the distance to the reconnection X-line is determined from cusp ion observations (see, Trattner et al. 2021a,b). Analysis of these events showed that the estimated location of the extended reconnection line was consistent with that predicted by the maximum magnetic shear model. Despite the estimated location of the reconnection line appearing along the magnetopause flank where the magnetosheath flow velocity may have been super-Alfvénic, the distance from the sampling spacecraft to the reconnection line was observed to be approximately constant over a span of several minutes.

2.6 Reconnection X-Lines Have a Variable, but Ordered Orientation

A primary extended reconnection line along the low- to mid-latitude dayside magnetopause includes a variety of orientations. These different orientations arise because such extended

reconnection X-lines include a mix of reconnection types. These extended X-lines include anti-parallel segments and, especially when a substantial IMF B_y component exists, a component reconnection X-line segment (with non-zero guide field) that is present within a few hours of local noon and intersects the anti-parallel segments along the magnetopause flanks. In general, the intersection between the component and anti-parallel segments of the extended reconnection X-line occurs strictly along the bridge ('saddle') of highest magnetic shear (see Fig. 2). Some deviations from this model are noted during narrow ranges of IMF clock angles ($\sim 120^\circ$ and $\sim 240^\circ$) (Trattner et al. 2018, 2021a) These deviations are a topic of ongoing research.

Varying orientations along an extended reconnection line are associated with a coordinate system oriented by magnetic field variance directions (e.g., the minimum variance analysis (MVA) (Sonnerup and Cahill 1967), minimization of faraday residue (MFR) (Khrabrov and Sonnerup 1998), and the maximum directional derivative of the magnetic field (MDDDB) (Shi et al. 2005)). A recent study by Fuselier et al. (2021) showed that when electron diffusion regions were sampled by the MMS spacecraft at the magnetopause along the component reconnection segment of the extended primary reconnection line, the component reconnection line was often oriented along the M-direction (intermediate variance direction). In contrast, when electron diffusion regions were sampled at the anti-parallel reconnection line locations, the large-scale reconnection line was composed of a series of X-lines that are stacked in a staircase fashion along the L-direction (direction of the reconnecting component of the magnetic field). The X-lines maintain the same orientation over long distances, with component X-lines and some anti-parallel X-lines maintaining orientation over many R_E and other anti-parallel X-lines maintaining orientation over at least 1 R_E .

2.7 Summary of Sect. 2

Reconnection at the dayside magnetopause initiates the Dungey cycle in the magnetosphere. Crucial to this initiation is reconnection at low latitudes, where previously closed magnetic field lines in the magnetosphere are opened. As originally depicted by Dungey (1963), the low latitude reconnection occurs when the IMF is southward. The newly opened field lines convect over the poles into the nightside. At the Earth's magnetopause, low-latitude reconnection occurs along long, quasi-continuous X-lines that extend across the entire dayside from the dawn terminator to the dusk terminator. These primary X-lines are quasi-stationary for quasi-steady IMF conditions. The reconnection rate may vary along these X-lines; however, it is not likely that it goes to zero for any extended period of time. The adjectives that describe reconnection X-lines at the magnetopause are summarized in Table 1.

The location and type of reconnection (component or anti-parallel) of these primary X-lines is well-described by the maximum magnetic shear model and recent studies using MMS have confirmed and extended this model. This empirically developed model uses only the IMF clock angle and cone angle to determine where reconnection occurs on the magnetopause. At the Earth's magnetopause (for southward IMF conditions), the IMF orientation alone controls the reconnection location because, over nearly the full range of solar wind conditions, there is no suppression of reconnection by diamagnetic effects.

3 Field Line Convection

3.1 Reconnection Jets and Convection

Once the magnetic fields of the Earth and solar wind are connected at the dayside X-line, "open" field lines are created. Since the extension of the open field line into the solar wind

Table 1 Adjectives that describe X-lines at the Earth's magnetopause and the definitions of these adjectives

Adjective	Meaning	Comparison to physical parameters	Observed Quantity
Primary	The main X-line at the magnetopause as opposed to secondary X-lines.	N/A	N/A
Long or Extended	Spatial extent of the X-line on the magnetopause.	Much longer than an ion skin depth: ~ 750 km at the magnetopause	Extending from $> 1 R_E$ to $> 10 R_E$ or > 10 to > 100 ion skin depths
Continuous or Quasi-continuous	Unbroken. Observations anywhere along the X-line yield similar meso-scale structure.	Continuous over lengths much longer than an ion skin depth	Quasi-continuous from $> 1 R_E$ to $> 10 R_E$ or > 10 to > 100 ion skin depths
Quasi-stationary	Remaining in approximately the same location under quasi-steady IMF conditions.	Remaining approximately in the same location for timescales longer than plasma convection times at the magnetopause: $\sim 1-2 R_E$ per minute	Quasi-stationary from \sim several minutes to > 10 minutes.
Quasi-steady	Reconnection rate variations along the X-line can be large, but do not go to zero.	Reconnection rate variability is not from zero to the maximum possible rate.	It is very difficult to quantify reconnection rate variations, but the rate does not go to zero over time periods of minutes to tens of minutes

travels away from the Sun at 300-800 km/s, magnetic tension pulls the field line across the dayside and slings it to the nightside, where it becomes an open tail lobe field line. This $\mathbf{J} \times \mathbf{B}$ force is well modeled by MHD models such as are available in the CCMC.

The ion jets from dayside reconnection partially precipitate into the atmosphere, creating a region called the “cusp”, or in some early papers, the “cleft” (Frank 1971; Heikkila and Winningham 1971). Since the particles are convecting tailward at the same time they are precipitating, this leads to an “ion cusp dispersion”, with the highest-energy ions precipitating first and thus most equatorward, and the progressively lower energy ions farther poleward (Shelley et al. 1976; Reiff et al. 1977). By examining the details of the particle cut-off energy, the distance to the X-line is determined (Cowley 1982) and the jet distribution reconstructed (Hill and Reiff 1977; Lockwood 1997). Occasionally an electron dispersion is observed between the last closed field line and the beginning of the ion dispersion (Burch et al. 1982). This electron dispersion is the ionospheric footprint of the electron edge of the low-latitude boundary layer at the magnetopause (Gosling et al. 1990).

The convection over the pole of reconnected field lines and reconnection in the tail produces a polar cap convection pattern depicted in Fig. 3 for purely southward IMF. This pattern is driven by the mapping of the solar wind electric field along field lines to the ionosphere as shown in Fig. 3. The dawn-to-dusk electric field (shown as a heavy red arrow) causes dayside-to-nightside $\mathbf{E} \times \mathbf{B}$ flow (shown as dashed lines) and produces the cross-polar cap potential. In principle, the cross-polar cap potential should be related to the length of the X-line or lines at the magnetopause. However, in practice, it is difficult to link the two quantities because of variations of the reconnection rate along the X-lines at the dayside and inefficiencies in plasma transfer on the flanks.

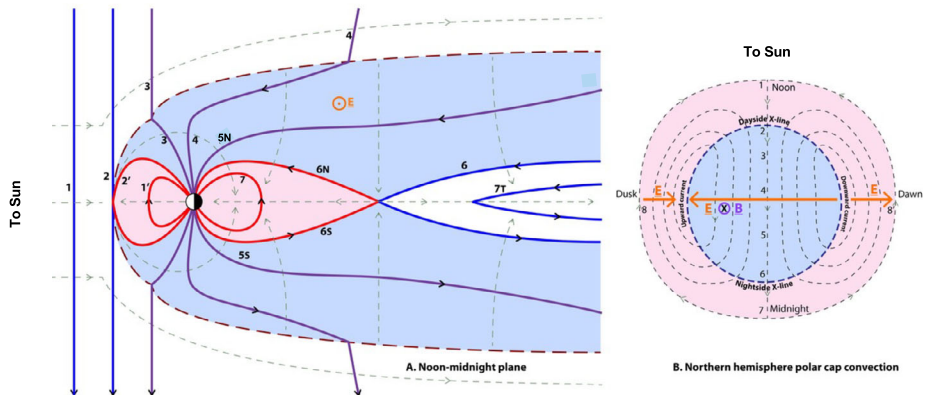


Fig. 3 (left panel) Simplified cross-section of the magnetosphere for due southward IMF. The bow shock and field line draping at the magnetopause were removed to illustrate the convection of a solar wind field line from noon to midnight. Solar wind field lines (blue, 1) reconnect at the magnetopause (2, 2') and form open field lines that convect over the poles (3, 4, 5N, 5S). In the tail, these field lines reconnect (6, 6N, 6S), forming closed field lines (7) earthward of the reconnection site. The closed field lines eventually return to the dayside. (right panel) The magnetopause reconnection, convection, tail reconnection, and the return of the field lines to the dayside produces a 2-cell convection pattern in the ionosphere. The footpoints of the field lines in the left panel are shown in the right panel

Continuing with the polar cap convection pattern in Fig. 3, magnetopause reconnection maps to the polar cap boundary near point 2, the field convects over the pole and through the polar cap from point 2 to point 6. Tail reconnection maps to the polar cap boundary near point 6. The polar cap flow continues equatorward and back sunward at lower latitudes. The sunward convecting field lines are closed and ultimately return to the dayside (point 8 and 8' back to point 1 in Fig. 3, with the return field lines not in the noon-midnight meridian cut in the left panel of Fig. 3). Ion outflow from the ionosphere occurs in the cusp, polar cap, and the nightside polar cap boundary.

When the X-line is not parallel to the equatorial plane on the dayside, as it frequently does for a strong non-zero Y-component of the IMF, the ionospheric outflow has a substantial downward or duskward flow component – typically reversed in the two hemispheres (Gonzalez and Mozer 1974). When IMF $B_y > 0$, the component reconnection X-line is tilted so that it is above the ecliptic on the duskside. Under these conditions, magnetic field lines convect downward and poleward and the cusp flow is downward in the northern hemisphere (e.g., Heelis 1984). The reverse is true in the Southern hemisphere or for $B_y < 0$.

The asymmetric flow also extends to the plasma mantle, the extension of the open field lines with cusp-like fluxes to the high latitude magnetotail. The mantle also exhibits a cusp ion dispersion, with the highest energy ions observed farthest from the magnetopause (Rosenbauer et al. 1975). Most of the plasma mantle is lost down the magnetotail (e.g., on field lines 5N and 5S in Fig. 3), leading to significant ionospheric escape (e.g., Schillings et al. 2020). The asymmetry of the convection means that the plasma mantle reaches the equatorial plane at lunar distance only on the favored (higher flow) side (Hardy et al. 1979). Only during times of very high convection is the magnetotail electric field intense enough that the plasma mantle reaches the near-earth neutral sheet. When this mantle flux reaches the neutral sheet during these extreme events, it participates in near-Earth reconnection (Reiff et al. 2016; see next section).

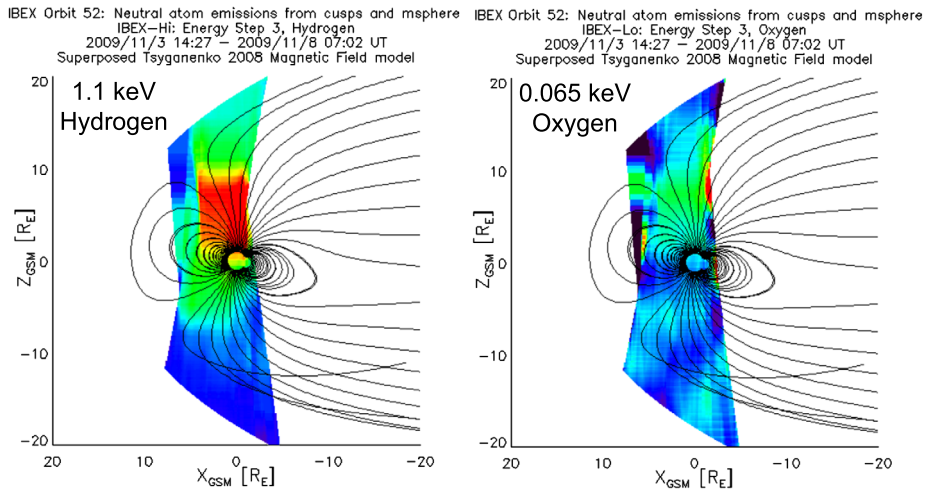


Fig. 4 ENA observations of the magnetosphere from the IBEX mission. The view is from the dusk side of the Earth and magnetic field lines are drawn from a magnetospheric magnetic field model to show the relationship of the ENA fluxes to the Earth's magnetospheric cusps. The left panel shows the precipitation of 1.1 keV hydrogen from the magnetosheath is asymmetric, with more precipitation occurring in the northern hemisphere cusp. The right panel shows that the 0.065 keV O^+ outflow from the ionosphere is also asymmetric with more outflow coming from the northern hemisphere cusp

3.2 Imaging the Cusp – Energetic Neutral Atoms

As solar wind protons enter the magnetosphere through reconnection and are accelerated along field lines with some precipitating in the Earth's magnetospheric cusps, a fraction of these ions charge exchange with the Earth's geocorona and become Energetic Neutral Atoms (ENAs). These ENAs are no longer bound to the Earth's magnetic field lines and propagate away from the Earth in all directions. Although the ENA flux is very low, it has been imaged by ENA cameras on the IMAGE mission (Burch 2000) and on the Interstellar Boundary Explorer (IBEX) mission (McComas et al. 2009). Figure 4 shows images of the Earth's magnetospheric cusps taken by the IBEX ENA cameras (Funsten et al. 2009; Fuselier et al. 2009). The left panel is an image of 1.1 keV Hydrogen, which images the entering magnetosheath population. The right panel is an image of 0.065 keV Oxygen, which images the ionospheric outflow population. The precipitation of magnetosheath ions into the cusp is asymmetric because the location of the reconnection X-line and the entering magnetosheath ion flux depends on dipole tilt (Petrinec et al. 2011). Figure 4 shows that the outflow is also asymmetric, with more O^+ outflow from the northern hemisphere than from the southern hemisphere. The origin of the O^+ outflow could be the cusp/cleft, or just the general auroral oval. The image is averaged over such a long period of time and does not have the spatial resolution to distinguish among these sources.

4 Magnetotail Plasma Sheet

4.1 Overview

As discussed in the previous three sections, magnetopause reconnection plays a crucial role in enabling energy and plasma from the solar wind to enter the magnetosphere. Furthermore,

as discussed in Sect. 3, the convection of reconnected field lines over the geomagnetic poles deposits this energy and plasma in the Earth's extended magnetotail. Also in Sect. 3, an additional particle source is the ionosphere, which populates tail lobes and plasma sheet, depending on presumably reconnection-related activity. The ultimate origin of this ionospheric plasma (i.e., the high latitude cusp, auroral oval, and polar cap) is a subject of ongoing study (e.g., Gloer et al. 2020; Kistler 2020; Toledo-Redondo et al. 2021a). Furthermore, the solar wind can also do work on the magnetosphere via compression and waves, thereby causing energy entry that does not directly involve reconnection. However, reconnection remains the dominant driving force in magnetospheric dynamics for southward IMF.

The plasma sheet may become populated directly by ionospheric particles and by plasma that enters through the low-latitude flanks, or indirectly via transport through the lobes, which is part of the Dungey cycle. The latter entry then requires magnetotail reconnection for the transport from the lobes to the plasma sheet. The relative importance of the different sources and entry mechanisms varies considerably depending particularly on distance along the tail and geomagnetic activity (e.g., Wing et al. 2014; Welling et al. 2015; Kistler 2020).

The Dungey cycle includes plasma transport from a nightside reconnection site toward and around the Earth to the dayside. Although the earthward transport from the nightside may be viewed as a quasi-steady process, it has been found to be inconsistent with adiabatic (i.e. entropy and mass conserving) transport (see Sect. 4.3).

The onset of reconnection in these events is apparently preceded by local current sheet thinning. The conditions that determine the location and extent of the thinning regions then are also responsible for the location of the reconnection sites. This section focuses on the global context. The local structure and plasma conditions of thin current sheets (TCSs) are discussed in Hwang et al. (2023, this collection).

Major consequences of reconnection are fast, Alfvénic, outflows. Earthward flow bursts are associated with locally enhanced northward magnetic fields and cross-tail electric fields, which are found to be the dominant mechanism to accelerate ions and electrons to suprathermal energies (see e.g., Phan et al. 2013; Oka et al. 2022; and Oka et al. 2023, this collection). Velocity shear and vorticity at the edges of the flows, particularly in their stopping and diversion region near Earth, are also a mechanism to twist and shear the magnetic field, building up field-aligned currents. These currents provide a connection to auroral streamers and, on larger scale, the substorm current wedge.

4.2 Sources and Entry

As pointed out above, there are two basic sources of plasma sheet particles, the ionosphere and the solar wind. Source differences are relevant for subsequent reconnection in the plasma sheet, as discussed in Chap. 1. Ionospheric ions enter the magnetotail in two ways (e.g., Kistler et al. 2019), either directly onto closed field lines through the auroral region or through the cusp onto open, lobe field lines. In the latter case, tail reconnection is necessary to trap these particles in the plasma sheet, similar to solar wind ions that enter from the lobes. During times of extreme polar cap potential drop, convection brings ionospheric O^+ through the tail lobes to become an accelerated population in the near-Earth plasma sheet (Reiff et al. 2016), as illustrated in Fig. 5.

As described in Sect. 1, for southward IMF solar wind plasma enters the magnetotail and eventually the plasma sheet predominantly by the dayside reconnection process.

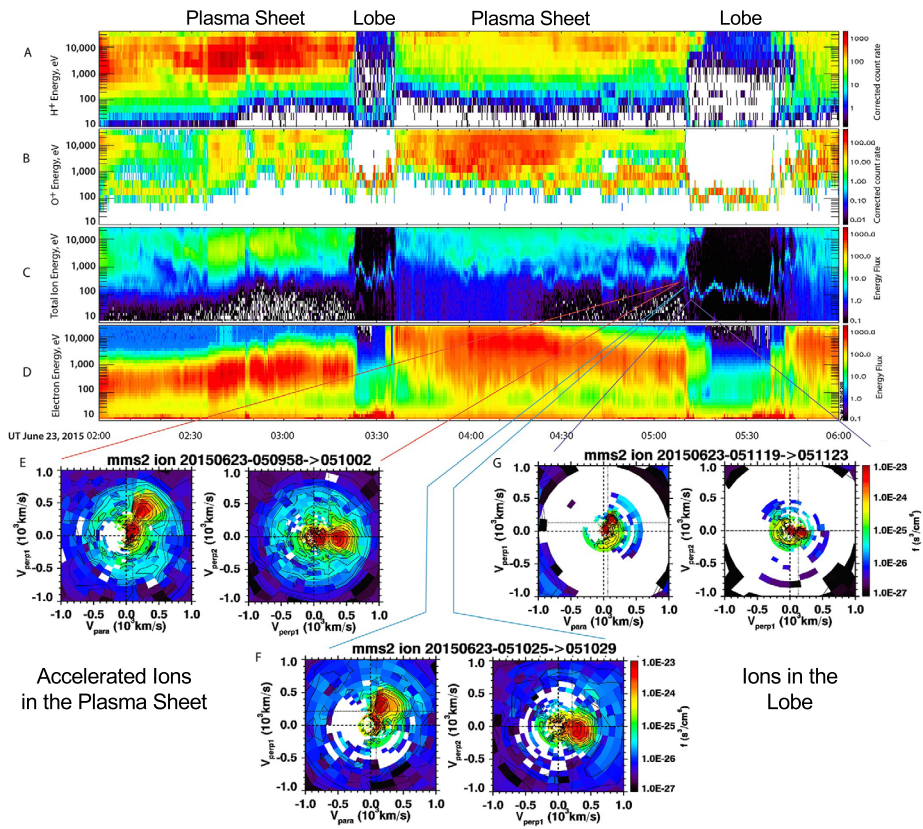


Fig. 5 HPCA (MMS1) and FPI (MMS2) measurements in the magnetotail from 0200 to 0600 on 23 June. (A) Energy spectrograms of the HPCA H⁺. Panel B shows an O⁺ beam from the ionosphere merging into the plasma sheet at each lobe/plasma sheet transition. FPI total ion and electron spectrograms of differential energy flux are shown respectively in Panels C and D, and clearly shows the transition from lobe conditions (virtually no fluxes except the O⁺ beam) to PSBL (where the energized lobe fluxes appear separate from the much more energetic plasma sheet fluxes). The bottom three panels (E, F and G) show three pairs of FPI distribution functions as the spacecraft exited the plasma sheet to the lobe. The left of each pair shows $v_{parallel}$ and v_{perp1} (along $\mathbf{E} \times \mathbf{B}$) components of the particle distribution functions, and the right of each pair shows the two perpendicular velocities, v_{perp1} and v_{perp2} . (From Reiff et al. 2016)

4.3 Transport

As briefly mentioned above, the earthward transport from a distant reconnection site, which is part of the Dungey cycle for southward IMF is visualized as a quasi-steady process within a steady magnetospheric magnetic field. However, Erickson and Wolf (1980) were the first to demonstrate that the average magnetotail configuration is inconsistent with adiabatic (i.e., entropy and mass conserving) transport from the distant to the near tail; such transport would lead to a pressure build-up in the near tail that is not observed and would not be balanced by the observed lobe magnetic pressure. Kivelson and Spence (1988) and Spence et al. (1989) then demonstrated that energy-dependent particle loss from cross-tail drifts may be sufficient only under very weak transport scenarios to reduce the pressure and solve this “pressure inconsistency.”

The obvious solution to this pressure inconsistency is the sporadic occurrence of reconnection in the near or mid tail, which reduces the particle and energy content of convecting closed magnetic flux tubes and adds buoyancy effects to the earthward transport (Pontius and Wolf 1990; Birn et al. 2009; Wolf et al. 2009). This conclusion is strongly supported by direct plasma sheet observations (Baumjohann et al. 1989, 1990; Angelopoulos et al. 1992), which have demonstrated that the major earthward transport in the near tail is accomplished by short-duration (~ 1 min) flow bursts, that may be grouped into ~ 10 min “bursty bulk flows” (BBFs), presumably driven by sporadic reconnection in the near- and mid-tail region or by interchange instabilities that allow rarified longitudinal sectors to enter while mass-loaded longitudinal sectors escape down the tail (Wolf et al. 2012; Sorathia et al. 2020).

4.4 Where and How Is Reconnection Initiated in the Near-Tail

The simple Dungey picture contains only one reconnection site (x -line) in the, presumably distant, tail. As pointed out above, a steady convection scenario would be inconsistent with observations and the dynamic tail is more consistent with sporadic reconnection events earthward of that site. Figure 6 shows the tail structure with two reconnection sites (x -lines), obtained from a data mining reconstruction technique, discussed further below (Sitnov et al. 2021). Where are these sites located, what is their cross-tail extent, and what determines their location and extent?

Zwickl et al. (1984) and Daly et al. (1984) used statistical analyses of ISEE-3 observations to show that strong, tailward bulk plasma flow becomes dominant in the distant ($r > 150 R_E$) plasma sheet. These tailward flows suggest the presence of a typical x -line location inside that distance; that has a tendency to move tailward after substorm onset (Baker et al. 1984). Fast flow observations at the Moon’s distance (Kiehas et al. 2018) indicated that frequently the distant neutral line is beyond $60 R_E$ downtail. Øieroset et al. (2000, 2001) identified a distant reconnection event near $60 R_E$. Occasionally, however, the distant x -line location may even move beyond $220 R_E$ (Schindler et al. 1989).

The location of the reconnection site in the near and mid tail may also vary considerably, being mostly between 20 and $30 R_E$ downtail and rarely inside of $20 R_E$ (Nagai et al. 1998; Nagai and Machida 1998). Indeed, for phase 2 of the MMS mission, the spacecraft apogee of $25 R_E$ (later raised to $29 R_E$) was chosen to maximize measurements in the region where near-tail reconnection most often occurs (Burch et al. 2016; Fuselier et al. 2016). It is not well known what determines this location and, prior to onset, the thinning of the current sheet, which enables the onset (McPherron et al. 1987; Pulkkinen et al. 1992; Sergeev et al. 1990; Sanny et al. 1994).

Nagai et al. (2005) used Geotail reconnection events to study the possible solar wind control of the radial distance of the magnetic reconnection site and found it likely that a higher efficiency of the energy input, measured by $V_x B_z$, rather than the total amount of energy input, affects this location. Magnetic reconnection was found to take place closer to the Earth when the energy input was more efficient. This is consistent with indications that reconnection occurs closer to Earth during storm-time substorms within a stressed magnetotail (Nagai 2021; see also Sect. 4.7).

The onset of reconnection is presumably preceded by the thinning of the tail current sheet to ion or sub-ion scale or, more likely, by the formation of a TCS embedded in the wider plasma sheet (for recent reviews, see Sitnov et al. 2019a,b; Runov et al. 2021). Birn and Schindler (2002) and Birn et al. (2004) demonstrated, through magnetostatic theory

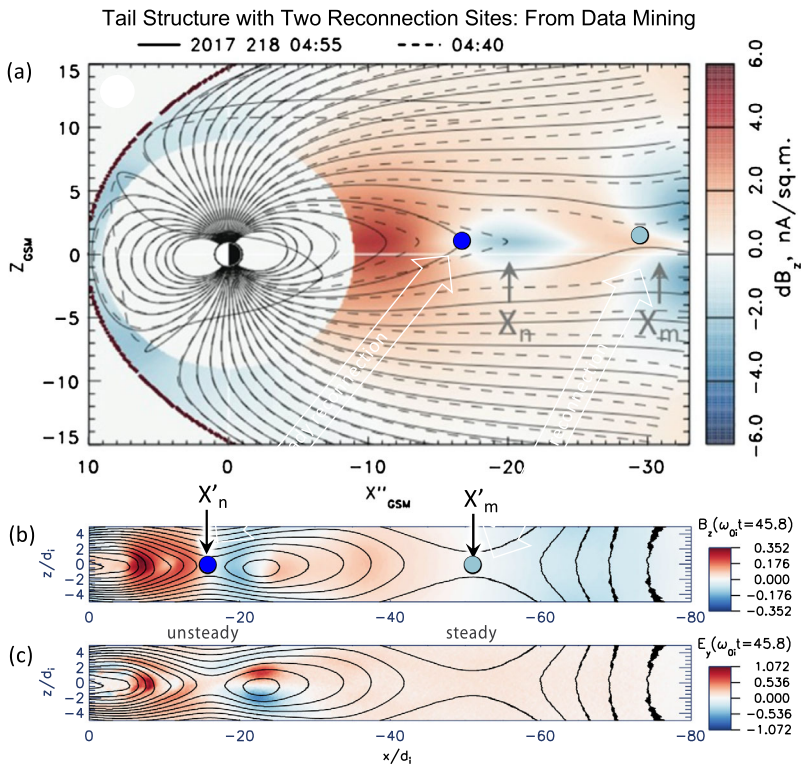


Fig. 6 (a) Regions of unsteady (X'_n) and steady (X'_m) reconnection in the data-mining reconstruction of the 6 August 2017 substorm shown by the meridional distribution of the normal magnetic field variation $dB_z = B_z(t_1) - B_z(t_0)$ with $t_0 = 04:40$ UT and $t_1 = 04:55$ UT; (b) Similar regions of unsteady (X'_n) and steady (X'_m) reconnection found in PIC simulations; (c) the distribution of the electric field E_y for the same PIC run; modified after Sitnov et al. 2021)

and MHD simulations, that high-latitude magnetopause boundary deformations, as expected from magnetic flux addition during the substorm growth phase, could cause the formation of local TCSs embedded in the wider tail plasma/current sheet. An alternative mechanism is based on enhanced equatorial plasma flow toward the dayside, which is part of the Dungey cycle (Hsieh and Otto 2014). This was shown to cause magnetic flux depletion at low latitudes, also leading to local current sheet thinning. Both mechanisms may operate together or at different times and different distances in the tail (Hsieh and Otto 2015; Gordeev et al. 2017).

High-latitude flux addition is consistent with an increase of the lobe field strength during the substorm growth phase, which is documented in many cases (e.g., McPherron 1972; Baker et al. 1996). It is also consistent with observational studies that indicate that substorm onset is more likely when the total open flux is increased (Kamide et al. 1977; Milan et al. 2009; Boakes et al. 2009; Lockwood et al. 2019). Specifically, Boakes et al. found that substorm onset was unlikely when the open flux was below 0.3 GWb, but increased linearly with increasing open flux above that value up to ~ 0.9 GWb, their observed maximum. This view is consistent with the role of the growth phase in the standard substorm model (Sect. 4.6). The models of TCS formation from high-latitude flux addition indicate a close relationship between thin current sheet formation (and hence substorm onset) and tail flaring

(see, also, Lockwood et al. 2019), which may be relevant for determining the location of TCS formation and reconnection onset.

In contrast, the low-latitude flux depletion does not require an increase in lobe field strength, which is also frequently observed (e.g., Petrukovich et al. 2000; Shukhtina et al. 2014). These results support the feasibility of both concepts. However, neither concept permits a direct and easy prediction of the location of the near-tail reconnection site from solar wind or other parameters.

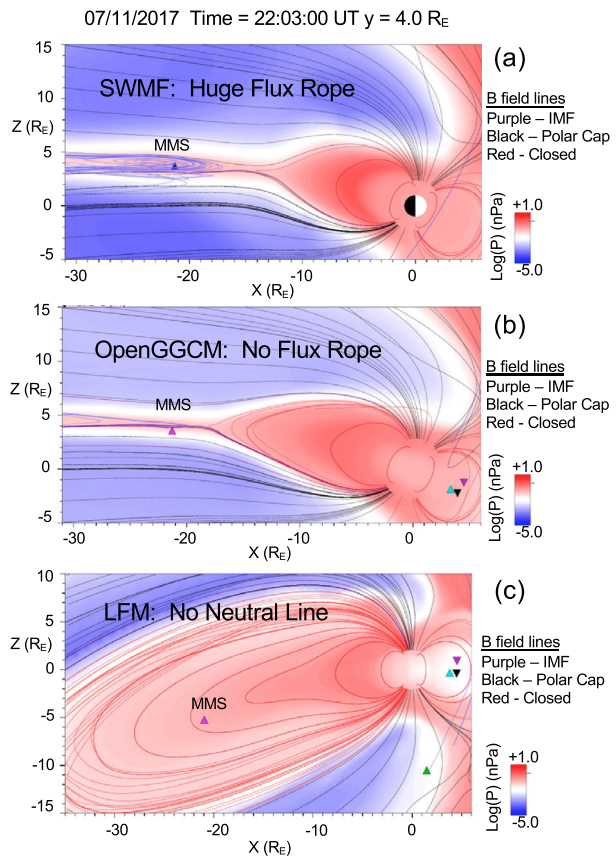
Other questions concern the downtail and cross-tail extent of the TCSs and subsequent reconnection. Artemyev et al. (2016b), found that current sheet thinning was associated with a strong radial pressure gradients $\partial p/\partial r$, indicating a short scale ($0.2 R_E$) along the current sheet that was comparable to the scale perpendicular to the sheet. At the other extreme, Artemyev et al. (2019) concluded from simultaneous observations in the near and distant tail that current sheet thinning occupies the entire tail from the near-Earth region down to lunar orbit. They also found that convergent plasma pressure gradients $\partial p/\partial y$, measured in equatorial thinning current sheets, indicated a localization of current sheet thinning near midnight. Such a concentration would be consistent with the estimated widths of earthward reconnection outflows of a few R_E (Nakamura et al. 2004)

One of the most puzzling findings of current sheet thinning prior to substorm onset is a collection of reports of an anti-correlation between plasma temperature and density, showing increases in density along with decreases in (both ion and electron) temperature (Artemyev et al. 2016a, 2019, 2021) during current sheet thinning. This trend had already been reported earlier by Huang et al. (1992), while a superposed epoch study by Baumjohann et al. (1991) did not indicate the existence of such a trend. A thermodynamic, e.g., isobaric, scenario that increases plasma density while reducing temperature in a single population (Birn et al. 1994) appears implausible. A more likely interpretation is that the satellites encounter different flux tubes carrying different plasma populations. This seems most plausible near the plasma sheet boundary where thinning brings different plasma populations equatorward combined with a compression. Most likely, the effect cannot be explained by just one plasma population but may involve, for instance, losses of higher-energy particles, which contribute more significantly to the temperature than to the density, or the inclusion of a cold particle population.

Another explanation of the temperature and density correlation is the formation of TCSs due to Speiser orbit effects (Sitnov et al. 2003). In this approach the current sheet thickness scales as the ion gyroradius in the lobe field, which is also close to the ion inertial length when the plasma anisotropy is small (Sitnov and Arnold 2022). The first scaling explains the decrease of the temperature, while the second matches the increase of the plasma density. Moreover, the first scaling is also consistent with the anticorrelation of the TCS thickness with the lobe field strength (e.g., Stephens et al. 2023, Fig. 4).

In principle, global simulations of the solar wind/magnetosphere system might be considered as the ideal tool to investigate the solar wind effect on the initiation of reconnection in the magnetotail. However, x-lines are often found to form too close to the Earth in these simulations (e.g., El-Alaoui et al. 2009; Park 2021). At present, it is not clear whether this is due to the missing non-MHD physics (e.g., Raeder et al. 1996) or to unavoidable numerical dissipation (e.g., Gonzalez and Parker 2016; Raeder 2022). In many of these models x-line formation and reconnection happen despite the absence of an explicit dissipation term in the MHD equations. Despite these deficiencies, large-scale MHD simulations have been highly successful in reproducing major global effects associated with substorms (see, e.g., Birn et al. 1996; Raeder 2003; Merkin et al. 2019), including the location of spacecraft relative to the X-line (Reiff et al. 2016; Torbert et al. 2018; Reiff et al. 2018).

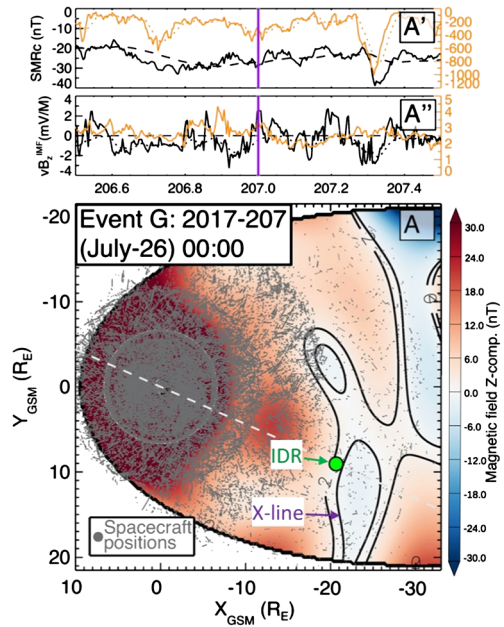
Fig. 7 Simulation results of an event on July 11, 2017, showing magnetic flux contours (solid black lines) and plasma pressure (color) on a logarithmic scale: (a) SWMF simulation in GSM coordinates, (b) OPENGGCM in GSM coordinates, and (c) LFM model in SM coordinates



Figures 7 (a, b, c) show frames from simulations of the July 11, 2017 tail reconnection event observed by MMS. The top figure (a) shows the SWMF simulation, which accurately predicted the MMS crossing the X-line a few minutes prior and predicted the huge flux rope which MMS observed. The middle simulation (b) shows the equivalent OpenGGCM model, which shows an extended neutral sheet but no flux rope; and (c) shows the same time using the LFM model which did not predict a near-earth neutral line at all.

Global simulations yield the evolution of X-lines and reconnection from an evolution driven by a time-dependent solar wind input. An alternative method relies on large statistical data bases of magnetospheric quantities (primarily magnetic fields) measured by satellite missions during varying driving and activity conditions. Reconstruction of the global structure from data is very challenging because of the data paucity with less than a dozen probes available for in-situ observations at any moment. However, modern machine-learning methods, and in particular, the “lazy-learning” approach based on mining multi-decade and multi-mission archives of geomagnetic field data using a nearest neighbor method combined with flexible magnetic field architectures using basis function expansions (Tsyganenko and Sitnov 2007; Sitnov et al. 2008; Stephens et al. 2019; see also Sect. 5 for more detail) have recently provided a breakthrough in this direction (Stephens et al. 2023). A key to the reconstruction has become the recurrent nature of storms and substorms, which allows one to enrich a few points of real observations available at the moment of interest with a super-constellation of up to 50,000 synthetic probes (shown by gray dots in Fig. 8).

Fig. 8 X-lines reconstructed for event G from the MMS library (Rogers et al. 2019, 2023) (green circle). Gray dots show $\sim 50,000$ historical data points used for the reconstruction of the field B_z (Stephens et al. 2023) assuming zero dipole angle. Top panels show global SuperMag indices SMR and SML (Gjerloev 2012) (SMRc is the pressure-corrected SMR (Tsyganenko et al. 2021)), vB_z IMF and solar wind dynamic pressure P_{dyn} . The MMS location is marked by the green circle



An example of reconstruction is shown in Fig. 8 for event G from the MMS library (Rogers et al. 2019, 2023). The x-line in the reconstructed field coincides closely with the reconnection site (ion diffusion region, IDR) identified by MMS. In total, 24 out of 26 reconstructed x- and o-lines ($B_z = 0$ contours) matched within $\sim 2R_E$ or nearly matched ($B_z = 2$ nT contours within $\sim 2 R_E$) the observed MMS IDR locations.

The data mining (DM) method predicts neutral line locations from finding nearest neighbors in parameter space based on five parameters. The parameter $V_x B_z$ directly describes solar wind input, whereas the others, given by the time-averaged Sym-H and its time derivative, as well as the AL index and its time-derivative, characterize storm and substorm dominated states that contain solar wind input only indirectly. The success of the DM method in predicting neutral line locations is surprising in view of the fact that none of these parameters has a direct obvious relationship to the location of the x-lines in the tail. Most recently, these empirical reconstructions have been merged with global MHD models using the explicit resistivity method (Hesse and Birn 1994) where DM “pointed” MHD to the data-derived X-line locations to nudge reconnection there (Arnold et al. 2023).

Through instantaneous fitting of sequences of configurations, the DM approach was also able to demonstrate the stretching and dipolarization during a substorm cycle (Stephens et al. 2019) with the formation of thin ion-scale current sheets embedded within the thicker plasma sheet (Sitnov et al. 2019b; Stephens et al. 2023).

4.5 Consequences of Magnetotail Reconnection: Flow Bursts, Particle Acceleration, Substorm Current Wedge, and Plasmod Formation

A direct consequence of magnetic reconnection is the conversion of magnetic energy into particle energy, which on fluid scales takes the form of plasma heating and fast bulk flows. On the earthward side of tail reconnection this is most prominent in the form of bursty bulk flows (BBFs, Angelopoulos et al. 1992), consisting of ~ 10 min fast flow periods of

hundreds of km/s with individual peaks of ~ 1 min duration (For recent reviews, see Sitnov et al. 2019a and Birn et al. 2021). Individual flow bursts tend to be associated with temporary enhancements of the (northward) magnetic field component B_z , which has led to denoting such an event dipolarizing flux bundle” (DFB, Liu et al. 2013a) or “flux pileup region” (FPR, Khotyaintsev et al. 2011). The enhanced B_z in combination with enhanced earthward flow also leads to an enhancement of the (predominantly duskward) electric field, which has led to the concept of “rapid flux transport” (RFT) events (Schödel et al. 2001).

When plasma is transported earthward from a distant reconnection site, particles are expected to become energized adiabatically; consistent with the shortening of magnetic flux tubes and the increase of the magnetic field strength. However, as pointed out above, there is little evidence that this happens in a quasi-steady fashion. Instead, sporadic reconnection events in the near and mid tail play the dominant role in energizing ions and electrons during their transport toward Earth, either in the vicinity of the reconnection site or within its exhaust regions. Numerous investigations based on observations, theory, and simulations have identified the, temporally and spatially localized, electric field of RFT events as the primary mechanism accelerating ions and electrons in the near tail to tens or hundreds of keV, and causing energetic particle “injections”, first documented by observations at geosynchronous orbit. This subject is discussed in more detail in Oka et al. (2023, this collection) (see also reviews by Birn et al. 2012, and Fu et al. 2020).

DFBs can also be the source of smaller-scale waves. Specifically, the sharp rise of B_z at the front of a DFB, the “dipolarization front” (DF), may drive lower-hybrid waves, and electron anisotropies in the accelerated population inside the DFB may be the cause of whistler waves. These effects are further discussed in Hwang et al. (2023, this collection).

The earthward flow from a near-tail reconnection site must be stopped closer to Earth and diverted azimuthally eastward and westward, consistent with the Dungey cycle. The flow shear and diversion distort the embedded magnetic field, causing twist and shear that is associated with field-aligned currents, which, in their simplest form flow toward the Earth on the dawn side and away on the dusk side. This paradigm was first developed on the basis of MHD simulations of near-tail reconnection (Birn and Hesse 1991; Scholer and Otto 1991). It is now the most widely accepted view of the build-up of the “substorm current wedge” (SCW), which also includes the closure of the field-aligned currents in the ionosphere through the auroral electrojet (McPherron et al. 1973; Keiling et al. 2009; Birn and Hesse 2014; Kepko et al. 2015).

This picture describes the build-up of the SCW. Once the magnetic field is distorted, the currents can continue to flow, maintained by overall force balance without further need of fast flows, until they are dissipated by ionospheric resistivity. Thus, fast flows typically have a duration of only a few minutes, while the wedge currents may persist for tens of minutes up to 1 hour. Individual flow bursts have been shown to be associated with wedge type currents (Sergeev et al. 1999, 2004; Nakamura et al. 2001a,b) but may collectively contribute as “wedgelets” to the total SCW (Liu et al. 2015; Birn et al. 2019; Merkin et al. 2019).

The major tailside consequence of near-tail reconnection is the severance and tailward ejection of a section of the plasma sheet, denoted as a plasmoid (Hones 1977). Plasmoids consist of loop-like magnetic field lines, which in a generalized 3D picture assume the form of a flux rope (Hughes and Sibeck 1987), some of which may include rather strong axial fields. Since plasmoids are consistent with transient reconnection, they are discussed in more detail in Sect. 7.

The original picture of plasmoids ejected tailward as simple entities is an oversimplification that has been modified by observations and simulations. They gain momentum by the accumulation of accelerated plasma with significant 3D variation (Hesse and Birn 1994).

Their speed may vary both along and across the tail; and some may even be stagnant (Nishida et al. 1986).

4.6 The Near-Earth Neutral Line Substorm Model

The formation of a new, temporary, reconnection site in the near tail is the core element of the neutral line model of substorms (Baker et al. 1996), also referred to as the near-Earth neutral line (NENL) model. Essential features were already formulated by Atkinson (1966) and summarized by Atkinson (1967):

a. The solar wind drags field lines from the region of closed field lines into the tail, either by viscous forces, or by the neutral-point mechanism proposed by Dungey (1958). There is a resulting increase in the tail magnetic field strength and a storing of potential energy.

b. The polar substorm begins when field lines recombine in an implosive fashion at the neutral sheet, in the manner indicated by Petschek (1964). This recombination implies the release of stored potential energy.

c. The recombined flux tubes are added to the night side of the closed region as a giant bulge, causing auroral effects.

d. The flux tubes flow around the closed region toward the day side, causing the magnetic substorm and further auroral effects.

Phase (a) obviously corresponds to the substorm “growth phase,” introduced by McPherron (1972) as part of a three-phase phenomenological model, consisting of growth phase, expansion phase and recovery phase (McPherron et al. 1973). Phase (b) represents the onset and phase (c) the expansion phase. Although this was not identified at the early time, phase (d) describes in fact the present view of the build-up of the substorm current wedge (Kepko et al. 2015), presented in Sect. 4.5. Further evidence and a detailed illustration that included a preexisting distant neutral line and the ejection of a plasmoid was then provided by Hones (1977). An updated view and more comprehensive discussions of the features of the NENL model including the context of modeling have been presented by Baker et al. (1996, 2016). The neutral line model represents the background for our understanding of large-scale substorm dynamics, particularly applied to isolated substorms. Some details, however, are still active areas of research, such as the potential role of ballooning/interchange instability prior to the onset of near-tail reconnection or in acceleration and providing cross-tail structure of magnetic flux tubes that are depleted by reconnection and plasmoid ejection (for a recent review, see Sitnov et al. 2019a,b).

4.7 Magnetotail Reconnection in Different Magnetospheric States

Both the solar wind driver and the pre-conditioning of the magnetosphere can modify the location and strength of reconnection in the near-Earth magnetotail (Nagai et al. 2005). The preconditioning, which involves the magnetic field configuration and the plasma sheet parameters, such as temperature, density, and ion composition, results not only from the solar wind history but also from coupling with the ionosphere. The pressure distribution in the magnetotail also affects where reconnection jets get diverted in the inner magnetotail (Dubyağın et al. 2010).

Various scenarios, in addition to isolated substorms, include magnetic storms, steady magnetospheric convection (SMC) events, periodic substorms and sawtooth events, as well as pseudo-breakups. The day/night flux transport and the location of reconnection differ in different magnetospheric states.

The most extreme cases are magnetic storms, occurring under strong solar wind driving conditions, which compress the magnetosphere and increase magnetosphere-ionosphere

coupling by enhanced energy deposition, also causing also enhanced ionospheric outflow of cold ions (Kronberg et al. 2021) and enhanced electric fields. Reconnection in storm time substorms can occur much closer to Earth (Miyashita et al. 2005; Angelopoulos et al. 2020) due to its compressed state.

Strong recurrent substorms during geomagnetic storms are called sawtooth events (STEs). They are associated with strong quasi-periodic energetic particle injections in the inner magnetosphere with recurrence times of 2–4 h (Borovsky et al. 1993; Borovsky and Yakymenko 2017). They are also likely related to solar wind Mach number (Lavaud and Borovsky 2008). STEs have a wider azimuthally extended injection region (Clauer et al. 2006; Henderson et al. 2006), a wider night-side ionospheric convection pattern, and a wider local time extent of dipolarization than isolated substorms (Cai et al. 2006a,b). This wider extent indicates also a wider cross-tail extent of the tail reconnection site, which tends to be located much closer to Earth than for isolated substorms (Henderson 2004), consistent with their storm-time occurrence.

In addition to the ~3h period STEs, substorm-like periodic activations with a ~1h period have been reported (e.g., McPherron and Chu 2018; Keiling et al. 2022), associated with dipolarizations, fast plasma flows and particle injections with the same periodicity. They are, however, not associated with storms and can occur over a wide range of AE values.

The mechanisms driving these periodic events are not well understood. For STEs, it might play a role that the nightside magnetosphere is much more stretched prior to the onset (Cai et al. 2006b). The approximate 3h waiting time might reflect an intrinsic oscillation period, assumed under strong driving (Huang et al. 2003; Borovsky and Yakymenko 2017). Global simulations with ionospheric outflow have suggested a possible role of stretching of the magnetotail from increased mass loading by O⁺ from the ionosphere, leading to an imbalance between day-night reconnection rates, which may result in a feedback loop in the magnetosphere-ionosphere system (Brambles et al. 2013; Ouellette et al. 2013).

Another possible mechanism driving periodic stretching and release relies on non-MHD effects, which arise from multi-scale modifications to a pure MHD approach, either by adding a physics-based dissipation term (Kuznetsova et al. 2007) or by including a locally embedded PIC simulation into a global MHD approach (Wang et al. 2022). Both approaches found consistency with a wider reconnection site in the tail, but with somewhat shorter sawtooth periods than observed: ~1.5 hrs (Kuznetsova et al. 2007) and 1.5 to 3 hrs (Wang et al. 2022). Wang et al. also reported weaker signatures at geosynchronous orbit and maximum magnetic field stretching near dawn and dusk rather than at local midnight.

These active events are in contrast to intervals called steady magnetospheric convection (SMC). SMCs are extended periods defined by quasi-steady solar wind input under southward IMF B_z, enhanced magnetospheric convection, but an absence of substorms. They are apparently governed by overall balance between dayside and nightside reconnection (e.g., DeJong and Clauer 2005). However, sporadic reconnection appears to happen in the mid tail with intermittent bursty flows (Sergeev et al. 1996), though the build-up of a high-pressure region in the inner magnetosphere prevents high-speed jets from penetrating into the inner magnetosphere (Kissinger et al. 2012).

DeJong et al. (2007) compared auroral features of isolated substorms, sawtooth, and SMC events and found that the polar cap oval measured during individual sawteeth contained, on average, 150% more magnetic flux than the oval measured during isolated substorms or SMC events. However, both isolated substorms and individual sawteeth showed a 30% decrease in polar cap magnetic flux during the dipolarization (expansion) phase, whereas the open polar flux remained steady in SMC events.

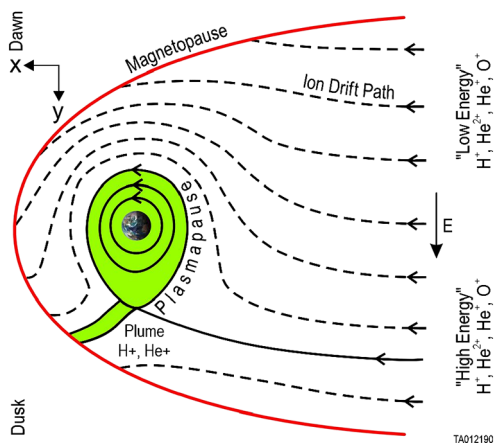


Fig. 9 After Toledo-Redondo et al. 2021 – Schematic of open and closed drift paths in the magnetosphere. Plasma of ionospheric (H^+ , He^+ , O^+) and solar wind (H^+ , He^{2+}) origin drift to the magnetopause in response to the cross-tail electric field and gradient and curvature drifts. In addition, a plasmaspheric plume (green-shaded extension of the plasmasphere) could intersect the magnetopause. After losses along their drift paths a fraction of ionospheric and solar wind ions and electrons re-encounter the magnetopause and complete the Dungey cycle

Pseudo-breakups are auroral brightenings, much like those at substorm initiation, with similar magnetospheric signatures such as dipolarization fronts, flow bursts, and field-aligned currents (Nakamura et al. 1994). Pseudo-breakups, however, do not develop substorm-like poleward auroral expansions. They may also occur during SMC events (De-Jong and Clauer 2005), consistent with small-scale energy releases but the absence of polar expansions. If the poleward expansion of aurora corresponds to tail reconnection proceeding into the lobes, then its absence would indicate that reconnection stops before reaching the lobes. Why reconnection stops before this point is obviously relevant for identifying conditions that stop or quench reconnection.

In summary, the dynamics in the Earth's magnetotail is driven by reconnection. In the original Dungey circulation model, this reconnection is steady and balances the dayside reconnection. However, observations for more than 50 years have shown that reconnection, especially in the near-tail distance of 20 – 30 R_E , is far from steady. Despite this unsteadiness, the Dungey circulation of magnetic flux is largely realized over timescales of hours.

5 Convection Back to the Dayside and the Completion of the Dungey Cycle

With near-tail reconnection, the plasma in the magnetotail is injected Earthward back into the inner magnetosphere. The paths ions take to return to the dayside depend on their energies. Lower energy ions are dominated by corotation and drift eastward while higher energy ions respond to gradient and curvature effects and drift westward to form the ring current (see, e.g., Kistler et al. 1989). Figure 9 shows a schematic of these drift paths that intersect the magnetopause, mostly sunward of the terminator. Fluxes and energies are not constant in this drift process. There are a variety of energy-dependent loss processes, including wave-particle interactions and charge exchange with the Earth's neutral hydrogen geocorona. The high-latitude ionosphere is a source of plasma throughout this convection, providing, for

example, the warm plasma cloak (Chappell et al. 2008) and a plasmaspheric plume (e.g., Carpenter et al. 1993), an extension of the plasmasphere (green-shaded region in Fig. 9) that extends to the dayside magnetopause over a limited range of local times during high magnetospheric activity. Thus, a small fraction of the solar wind plasma that entered on the dayside and injected ionospheric plasma from the high latitude ionosphere ultimately returns to the magnetopause and completes the Dungey cycle.

6 The Dungey Cycle for Northward IMF and Near-Radial IMF

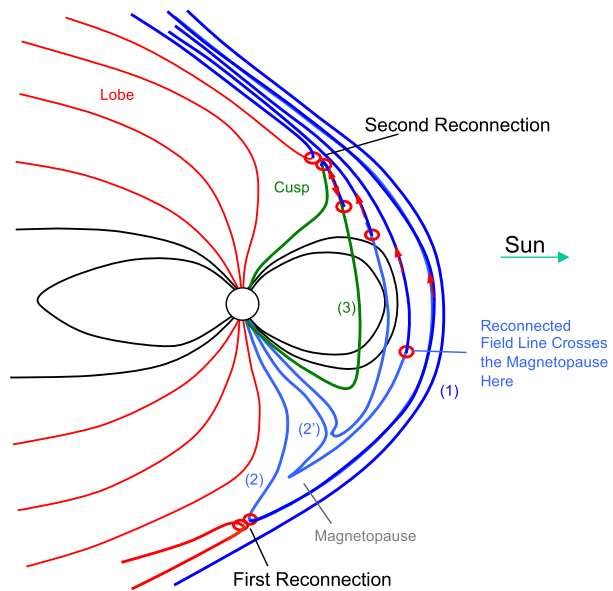
6.1 Northward IMF

The previous 5 sections outline the important role of reconnection in the Dungey cycle when the IMF is southward. Reconnection also plays an important role in magnetospheric dynamics when the IMF is northward (see the recent review by Lavraud and Trattner (2021)). Under such conditions, Dungey (1963) originally proposed that reconnection would occur at the magnetopause on magnetospheric field lines poleward of the cusps. In his original, 2-dimensional diagram, reconnection occurs simultaneously poleward of both cusps between magnetosheath and lobe field lines in both hemispheres. This type of reconnection is called dual-lobe reconnection. In 3-dimensions, and with dipole tilt and a finite B_Y component of the IMF, the reconnection is not simultaneous and can also occur on high-latitude, non-lobe field lines in either hemisphere (e.g., Lavraud et al. 2005, 2006; Fuselier et al. 2014; Lavraud et al. 2018). In particular, Lavraud et al. (2005) showed through statistical analysis that dipole tilt determines which hemisphere high-latitude reconnection occurs first, but it does not rule out dual-lobe reconnection. Figure 10 shows non-simultaneous dual-lobe reconnection and the consequences for field line topology and convection (Fuselier et al. 2012). Magnetosheath field lines (dark blue) reconnect first in the southern hemisphere poleward of the cusp. Under the tension force, these open field lines snap sunward and dawnward. The small red circles show where the field lines cross the magnetopause. As the field lines convect dawnward and drape against the magnetopause, they reconnect a second time poleward of the northern cusp, forming closed field lines inside the magnetosphere on the dayside. These field lines are filled with magnetosheath plasma and, because ionospheric outflow from the cusp also occurs along these field lines, they are filled with ionospheric plasma as well (Fuselier et al. 1989, 2019a).

Thus, just as for southward IMF, the Dungey cycle for northward IMF starts with reconnection at the dayside magnetopause. This reconnection produces a boundary layer on the dayside all the time (Fuselier et al. 1995; Øieroset et al. 2008) and has been observed as a quasi-steady process for northward IMF intervals that last for hours (Frey et al. 2003). Unlike southward IMF, the reconnection X-line poleward of the cusps does not extend over the entire dayside magnetopause (Fuselier et al. 2002). Furthermore, this mass-loaded field line convects slowly around the flanks of the magnetosphere rather than relatively rapidly over the poles for southward IMF. Similarly, there is a very slow transfer of magnetic flux to the nightside when the IMF is northward.

The convection of mass-loaded field lines on the flanks of the magnetopause under northward IMF conditions opens the possibility of additional magnetosheath plasma entry into the magnetosphere by the Kelvin-Helmholtz Instability (KHI), (e.g., Otto and Fairfield 2000; Nykyri and Otto 2001; Nykyri et al. 2006, 2021). The wound-up KH vortices are subject to local reconnection. This type of reconnection has been studied extensively for one MMS KHI event (Eriksson et al. 2016; Vernisse et al. 2016; Li et al. 2016). KH modes corrugate

Fig. 10 After Fuselier et al. (2012) – Three-dimensional reconstruction scenario. Magnetosheath field lines (1) reconnect poleward of the southern cusp forming field lines 2 and 2'. In the vicinity of the reconnection sites, these field lines convect sunward and downward. The points where they cross the magnetopause (small red circles) move northward and downward. At some later time, when the field line has convected away from the dayside magnetopause, a second reconnection occurs. This reconnection poleward of the northern hemisphere cusp on the part of the field line that is still in the magnetosheath forms the newly closed field line 3



the low-latitude magnetopause and enable reconnection between plasma sheet and magnetosheath, which traps magnetosheath plasma. These combined KH and reconnection plasma entry mechanisms help populate the plasma sheet on the flanks, with subsequent drift necessary to transport particles toward the center (e.g., Lavraud and Trattner 2021).

When the IMF is northward, high-latitude reconnection and plasma entry on the flanks are manifested in the plasma convection in the cusp and the convection cells in the high latitude ionosphere. The cusp ion dispersion is observed to be “reversed”, with higher energy ions at the most poleward latitudes instead of the opposite for southward IMF conditions. Initially, this reversed convection was thought to be a consequence of diffusive entry at the magnetopause; however, it is now well established that the reverse dispersion is a consequence of high latitude reconnection and sunward convection of reconnected field lines (Burch et al. 1980). Imaging of the cusp footprint in the ionosphere, combined with simultaneous in situ observations of reconnection at high latitudes has firmly established this connection between the magnetopause and cusp (Phan et al. 2003). Furthermore, this same imaging has established that the reconnection is quasi-steady and present all the time under northward IMF conditions (Frey et al. 2003).

For northward IMF, magnetosheath particle fluxes from reconnection and Kelvin-Helmholtz entry are observed at low latitudes on the flanks in a relatively wide boundary layer of antisunward flowing plasma. In the ionosphere, the result of this combined reconnection and KH entry is a “four cell” convection pattern. The two cells at high latitude have sunward flow in the central polar cap from lobe reconnection (Burke et al. 1979).

In the magnetotail, there is a distant reconnection site that persists for northward IMF. Cross-tail particle transport typically requires curvature and gradient drifts that exceed earthward $\mathbf{E} \times \mathbf{B}$ drifts, which becomes more effective at higher energies and southward IMF conditions. However, azimuthal flux transport in the magnetotail has been identified also when the IMF is northward and there is significant IMF B_y . Under these conditions the effects of northward IMF were sufficiently weak so that the Dungey-cycle twin-vortex convection observed for southward IMF was still maintained albeit with high asymmetry (Grocott et al.

2003, 2007). Since these events, apparently driven by reconnection at a distant site, did not exhibit substorm signatures they were called “tail reconnection during IMF-northward, non-substorm intervals” (TRINNIIs) (Milan et al. 2005).

While these TRINNI intervals apparently lack near-Earth reconnection, substorms exist also during northward IMF intervals (Lee et al. 2010; Peng et al. 2013), indicating that the onset of near-Earth reconnection does not have to be directly associated with enhanced dayside reconnection and can dissipate previously stored magnetotail energy. However, Peng et al. (2013) found that these substorms occurred mostly soon after southward IMF B_z periods and that intense substorms occurred only during relatively brief northward IMF B_z intervals. These observations suggest that southward IMF is still needed for the strong buildup of flux in the tail and it remains an open question what triggers those events during northward IMF.

In summary, northward IMF also produces a Dungey-like cycle. Magnetic reconnection at the magnetopause initiates this cycle and the persistent, distant tail reconnection site returns plasma sunward. However, the convection from the dayside to the nightside around the flanks of the magnetopause is considerably slower and weaker than the convection over the poles for southward IMF. Magnetic flux buildup in the magnetotail is much weaker and, as long as the northward IMF conditions persist, it is not clear if there is sufficient near-Earth reconnection to transfer plasma back to the dayside to complete the Dungey cycle.

6.2 Near-Radial IMF

IMF-cone angles $<25^\circ$ or $>155^\circ$ occur $\sim 15\%$ of the time at 1 AU (e.g., Pi et al. 2014). During these times of near-radial IMF, the quasi-parallel bow shock is upstream of the subsolar magnetopause. Turbulence generated at and upstream of the bow shock convects downstream and creates significant fluctuations in the plasma and magnetic field magnitude and orientation. Searching for signatures of reconnection at the magnetopause under these conditions is difficult. Furthermore, the magnetosheath draping model used in the maximum magnetic shear model is not valid for these cone angles and the location of the reconnection X-line is uncertain. Nonetheless, signatures of reconnection have been observed under these cone angle conditions, although the steadiness of this reconnection is questionable (e.g., Walsh et al. 2017; Toledo-Redondo et al. 2021b). One promising line of work is the use of large spacecraft datasets to construct a new generation of data-driven field line draping maps, with the potential to improve predictions of magnetic field orientation at the magnetopause (Michotte de Welle et al. 2022).

However, significantly more work is needed to understand how the Dungey cycle is affected by near-radial IMF conditions.

7 Multiple, Transient Reconnection on a Global Scale and Modifications to the Dungey Cycle

Reconnection plays critical roles in the Dungey cycle. Up to this point, there has been no discussion of variability in reconnection at the dayside magnetopause and very little discussion about reconnection variability in the tail. For southward IMF, there are long, primary X-lines at the dayside magnetopause. These primary X-lines are quasi-stationary and quasi-steady (Fuselier et al. 2019b). For quasi-steady reconnection, the reconnection rate does not go to zero over long periods of time as long as the direction of the IMF is also relatively

steady. The rate could vary by large amounts within this long time period, which is why the rate is described as quasi-steady.

There is also considerable evidence for transient reconnection at the magnetopause. The original model for flux transfer events (FTEs) is transient in both space and time (Russell and Elphic 1978). FTEs have been modeled also as bulges on the magnetopause between two active reconnection X-lines (Lee and Fu 1986). There is ample evidence of multiple X-lines at the dayside magnetopause (e.g., Hasegawa et al. 2010; Vines et al. 2017; Russell et al. 2017; Trattner et al. 2012; Fuselier et al. 2018, 2022). Some observations are interpreted in terms of a model where there is a quasi-stationary, primary reconnection X-line at the magnetopause and a temporally and/or spatially variable, secondary reconnection X-line separated by up to several R_E (Fuselier et al. 2018, 2022). Thus, there is both quasi-steady and transient reconnection co-existing at the magnetopause for southward IMF.

Multiple X-lines at the magnetopause are manifested in the cusp as overlapping ion dispersions (Fuselier et al. 1997; Lockwood 1995; Onsager et al. 1995; Trattner et al. 1998, 2012). For single reconnection, the precipitating magnetosheath ions disperse in the cusp such that the highest energy ions are observed at the lowest latitude. Overlapping ion dispersions have two (or more) of these dispersions separated in time. The separation provides information on the spacing of the two (or more) reconnection sites at the magnetopause. Recently, observations at the magnetopause and in the cusp have demonstrated the connection between multiple X-lines at the magnetopause and overlapping dispersions in the cusp. An open question about this connection is why multiple X-lines at the magnetopause seem to be common, but overlapping dispersions in the cusp do not appear to be that common (e.g., Trattner et al. 1998).

Multiple X-lines and transient reconnection also occur in the magnetotail. As discussed in Sect. 4.6, the formation of a new, temporary, reconnection site in the near tail is the core element of the neutral line model of substorms. Thus, the magnetotail part of the global Dungey cycle relies on transient reconnection. However, plasma observations both earthward and tailward of the temporary reconnection site indicate temporal and spatial variability on timescales much shorter than the substorm timescale of hours and much smaller than the ~ 20 – $40 R_E$ longitudinal extent of the near-Earth magnetotail.

On the earthward side of the near-Earth reconnection site, plasma flows are intrinsically bursty (BBFs Angelopoulos et al. 1992) and may carry embedded small-scale magnetic island or flux rope structures (e.g., Slavin et al. 2003). Observations in the magnetotail suggest that such near-Earth reconnection sites are activated multiple times at different locations (Nakamura et al. 2011), suggesting that multiple transient reconnection sites are likely key to understanding longer time-scale and larger spatial-scale magnetotail responses related to the Dungey cycle. On the tailward side, large plasmoids typically have multiple-island substructures (e.g., Hones et al. 1984), while scale sizes along the Sun-Earth direction may vary between more than $100 R_E$ (Hones et al. 1984), several R_E (Moldwin and Hughes 1992; Slavin et al. 2003) and even shorter scales of a few ion inertial lengths (Sun et al. 2019). Two-point measurements at the Moon's distance indicate a cross-tail size of 5–10 R_E . The cross-tail size increases with stronger activity measured by the auroral electrojet, or AE index (Li et al. 2014); however, this cross-tail size is still a fraction of the cross-tail extent of the magnetotail.

The focus of this section has been on the global scale and global consequences of transient reconnection. Transient reconnection produces a wealth of phenomena on the meso- and micro-scale that is considered in much more detail in Hwang et al. (2023, this collection).

8 Conclusions

In summary, this article discusses global-scale structure and consequences of reconnection, conveniently organized around the Dungey Cycle. Magnetic reconnection at the dayside magnetopause and in the magnetotail are clearly the drivers of the global Dungey cycle for southward IMF. The recent advances in the global structure and consequences of reconnection from the MMS mission and modeling include a detailed understanding of the location and steadiness of reconnection at the dayside magnetopause and in the magnetotail and the importance of multiple plasma sources. There are important questions about global reconnection that remain. These questions focus on 1) magnetosheath plasma entry into the magnetosphere and magnetotail dynamics when the IMF is northward and 2) how multiple reconnection and reconnection variability at the magnetopause and in the magnetotail fit into and complicate the classic Dungey Cycle picture of global magnetospheric circulation.

Acknowledgements The authors thank the International Space Science Institute (ISSI) for hosting the Magnetic Reconnection: Explosive Energy Conversion in Space Plasmas team. The MMS mission has been a tremendous success, and the many women and men that helped create this mission share in this success.

Funding Open Access funding provided thanks to the CRUE-CSIC agreement with Springer Nature. Research at Southwest Research Institute is funded by the NASA MMS prime contract NNG04EB99C. Research at LASP is supported by NASA grant NNG04EB99C and 80NSSC20K0688. Research at Lockheed Martin is supported by NASA grant 80NSSC18K1379 and MMS subcontract 499935Q. Research at the University of Murcia is supported by MCIN/AEI/PRTR 10.13039/501100011033 (grants PID2020-112805GA-I00 and TED2021-129357A-I00) and Seneca Agency from Region of Murcia (grant 21910/PI/22). Research at Imperial College London is supported by UKRI(STFC) grant ST/001071/1.

Declarations

Competing Interests The authors declare that they have no conflicts of interest.

Open Access This article is licensed under a Creative Commons Attribution 4.0 International License, which permits use, sharing, adaptation, distribution and reproduction in any medium or format, as long as you give appropriate credit to the original author(s) and the source, provide a link to the Creative Commons licence, and indicate if changes were made. The images or other third party material in this article are included in the article's Creative Commons licence, unless indicated otherwise in a credit line to the material. If material is not included in the article's Creative Commons licence and your intended use is not permitted by statutory regulation or exceeds the permitted use, you will need to obtain permission directly from the copyright holder. To view a copy of this licence, visit <http://creativecommons.org/licenses/by/4.0/>.

References

- Alexeev II, Sibeck DG, Bobrovnikov SY (1998) Concerning the location of magnetopause merging as a function of the magnetopause current strength. *J Geophys Res* 103(A4):6675–6684. <https://doi.org/10.1029/97JA02863>
- Angelopoulos V, Baumjohann W, Kennel CF, Coroniti FV, Kivelson MG, Pellat R et al (1992) Bursty bulk flows in the inner central plasma sheet. *J Geophys Res* 97:4027–4039
- Angelopoulos V, Artemyev A, Phan TD et al (2020) Near-Earth magnetotail reconnection powers space storms. *Nat Phys* 16:317–321. <https://doi.org/10.1038/s41567-019-0749-4>
- Arnold H, Sorathia K, Stephens G, Sitnov M, Merkin VG, Birn J (2023) Data mining inspired localized resistivity in global MHD simulations of the magnetosphere. *J Geophys Res* 128:e2022JA030990. <https://doi.org/10.1029/2022JA030990>
- Artemyev AV, Angelopoulos V, Runov A (2016a) On the radial force balance in the quiet time magnetotail current sheet. *J Geophys Res* 121:4017–4026. <https://doi.org/10.1002/2016JA022480>
- Artemyev AV, Angelopoulos V, Runov A, Petrokovich AA (2016b) Properties of current sheet thinning at $x \sim -10$ to $-12 R_E$. *J Geophys Res* 121:6718–6731. <https://doi.org/10.1002/2016JA022779>

- Artemyev AV, Angelopoulos V, Runov A, Petrukovich AA (2019) Global view of current sheet thinning: plasma pressure gradients and large-scale currents. *J Geophys Res* 124:264–278. <https://doi.org/10.1029/2018JA026113>
- Atkinson G (1966) A theory of polar substorms. *J Geophys Res* 71:5157–5164
- Atkinson G (1967) Polar magnetic substorms. *J Geophys Res* 72:1491–1494
- Atz EA, Walsh BM, Broll JM, Zou Y (2022) The spatial extent of magnetopause magnetic reconnection from in situ THEMIS measurements. *J Geophys Res* 127:e2022JA030894. <https://doi.org/10.1029/2022JA030894>
- Baker DN, Bame SJ, Birn J, Feldman WC, Gosling JT, Hones EW Jr, Zwickl RD, Slavin JA, Smith EJ, Tsurutani BT, Sibeck DG (1984) Direct observations of passages of the distant neutral line (80–140 R_E) following substorm onsets: ISEE-3. *Geophys Res Lett* 11:1042
- Baker DN, Pulkkinen TI, Angelopoulos V, Baumjohann W, McPherron RL (1996) Neutral line model of substorms: past results and present view. *J Geophys Res* 101(A6):12975–13010. <https://doi.org/10.1029/95JA03753>
- Baker DN et al (2016) A telescopic and microscopic examination of acceleration in the June 2015 geomagnetic storm: magnetospheric multiscale and Van Allen Probes study of substorm particle injection. *Geophys Res Lett* 43:6051–6059. <https://doi.org/10.1002/2016GL069643>
- Baumjohann W, Paschmann G, Sckopke N, Cattell CA (1989) Average plasma properties in the central plasma sheet. *J Geophys Res* 94(A6):6597–6606. <https://doi.org/10.1029/JA094iA06p06597>
- Baumjohann W, Paschmann G, Lühr H (1990) Characteristics of high-speed flows in the plasma sheet. *J Geophys Res* 95:3801–3809
- Baumjohann W, Paschmann G, Nagai T, Lühr H (1991) Superposed epoch analysis of the substorm plasma sheet. *J Geophys Res* 96:11605
- Berchem J, Fuselier SA, Petrinc S, Frey HU, Burch JL (2003) Dayside proton aurora: comparisons between global MHD simulations and IMAGE observations. *Space Sci Rev* 109:313–349. <https://doi.org/10.1023/B:SPAC.0000007523.23002.92>
- Birn J, Hesse M (1991) The substorm current wedge and field-aligned currents in MHD simulations of magnetotail reconnection. *J Geophys Res* 96:1611
- Birn J, Hesse M (2014) The substorm current wedge: Further insights from MHD simulations. *J Geophys Res* 114. <https://doi.org/10.1002/2014JA019863>
- Birn J, Schindler K (2002) Thin current sheets in the magnetotail and the loss of equilibrium. *J Geophys Res* 107(A7):SMP18. <https://doi.org/10.1029/2001JA0291>
- Birn J, Schindler K, Janicke L, Hesse M (1994) Magnetotail dynamics under isobaric constraints. *J Geophys Res* 99:14863
- Birn J, Hesse M, Schindler K (1996) MHD simulations of magnetotail dynamics. *J Geophys Res* 101:12939–12954
- Birn J, Dorelli JC, Schindler K, Hesse M (2004) Thin current sheets and loss of equilibrium: three-dimensional theory and simulations. *J Geophys Res* 109:A02215. <https://doi.org/10.1029/2003JA010275>
- Birn J, Hesse M, Schindler K, Zaharia S (2009) Role of entropy in magnetotail dynamics. *J Geophys Res* 114. <https://doi.org/10.1029/2008JA014015>
- Birn J, Artemyev AV, Baker DN, Echim M, Hoshino M, Zelenyi LM (2012) Particle acceleration in the magnetotail and aurora. *Space Sci Rev* 173:49–102. <https://doi.org/10.1007/s11214-012-9874-4>
- Birn J, Liu J, Runov A, Kepko L, Angelopoulos V (2019) On the contribution of polarized flux bundles to the substorm current wedge and to flux and energy transport. *J Geophys Res* 124:5408–5420. <https://doi.org/10.1029/2019JA026658>
- Birn J, Runov A, Khotyaintsev Y (2021) Magnetotail processes. In: Maggiolo R, André N, Hasegawa H, Welling DT (eds) *Space physics and aeronomy collection volume 2: magnetospheres in the Solar System*, 1st edn. Geophysical monograph, vol 259. Am. Geophys. Union, Washington. <https://doi.org/10.1002/9781119815624.ch17>
- Boakes PD, Milan SE, Abel GA, Freeman MP, Chisham G, Hubert B (2009) A statistical study of the open magnetic flux content of the magnetosphere at the time of substorm onset. *Geophys Res Lett* 36:L04105. <https://doi.org/10.1029/2008GL037059>
- Borovsky JE (2008) The rudiments of a theory of solar wind/magnetosphere coupling derived from first principles. *J Geophys Res* 113. <https://doi.org/10.1029/2007JA012646>
- Borovsky JE (2013) Physical improvements to the solar wind reconnection control function for the Earth's magnetosphere. *J Geophys Res* 118:2113–2121. <https://doi.org/10.1002/jgra.5011>
- Borovsky JE, Yakymenko K (2017) Substorm occurrence rates, substorm recurrence times, and solar wind structure. *J Geophys Res* 122:2973–2998. <https://doi.org/10.1002/2016JA023625>
- Borovsky JE, Nemzek RJ, Belian RD (1993) The occurrence rate of magnetospheric-substorm onsets: random and periodic substorms. *J Geophys Res* 98:3807–3813. <https://doi.org/10.1029/92JA02556>

- Brambles OJ, Lotko W, Zhang B, Ouellette J, Lyon J, Wiltberger M (2013) The effects of ionospheric outflow on ICME and SIR driven sawtooth events. *J Geophys Res* 118:6026–6041. <https://doi.org/10.1002/jgra.50522>
- Burch JL (2000) IMAGE mission overview. *Space Sci Rev* 91:1–14. <https://doi.org/10.1023/A:1005245323115>
- Burch JL, Reiff PH, Spiro RW, Heelis RA, Fields SA (1980) Cusp region particle precipitation and ion convection for northward interplanetary magnetic field. *Geophys Res Lett* 7:393–396
- Burch JL, Reiff PH, Heelis RA, Winningham JD, Hanson WB, Gurgioli C, Menietti JD, Hoffman RA, Barfield JN (1982) Plasma injection and transport in the mid-altitude polar cusp. *Geophys Res Lett* 9:921–924. <https://doi.org/10.1029/GL009i009p00921>
- Burch JL, Moore TE, Torbert RB et al (2016) Magnetospheric multiscale overview and science objectives. *Space Sci Rev* 199:5–21. <https://doi.org/10.1007/s11214-015-0164-9>
- Burke WJ, Kelley MC, Sagalyn RC, Smiddy M, Lai ST (1979) Polar cap electric field structures with a northward interplanetary magnetic field. *Geophys Res Lett* 6:21–24
- Cai X, Clauer CR, Ridley AJ (2006a) Statistical analysis of ionospheric potential patterns for isolated substorms and sawtooth events. *Ann Geophys* 24:1977–1991. <https://doi.org/10.5194/angeo-24-1977-2006>
- Cai X, Henderson MG, Clauer CR (2006b) A statistical study of magneticepolarizationn for sawtooth events and isolated substorms at geosynchronous orbit with GOES data. *Ann Geophys* 24:3481–3490. <https://doi.org/10.5194/angeo-24-3481-2006>
- Carpenter DL, Giles BL, Chappell CR, Decreau PME, Anderson RR, Persoon AM, Smith AJ, Corcuff Y, Canu P (1993) Plasmasphere dynamics in the duskside bulge region: a new look at an old topic. *J Geophys Res* 98:19243
- Cassak PA, Fuselier SA (2016) Reconnection at Earth's dayside magnetopause. In: Gonzalez W, Parker E (eds) *Magnetic reconnection. Astrophysics and space science library*, vol 427. Springer, Cham, pp 213–276. <https://doi.org/10.1007/978-3-319-26432-5>
- Chappell CR, Huddleston MM, Moore TE, Giles BL, Delcourt DC (2008) Observations of the warm plasma cloak and an explanation of its formation in the magnetosphere. *J Geophys Res* 113:A09206. <https://doi.org/10.1029/2007JA012945>
- Clauer CR, Cai X, Welling D, DeJong A, Henderson MG (2006) Characterizing the 18 April 2002 storm-time sawtooth events using ground magnetic data. *J Geophys Res* 111:A04S90. <https://doi.org/10.1029/2005JA011099>
- Coppi B, Mark JWK, Sugiyama L, Bertin G (1979) Reconnecting modes in collisionless plasmas. *Phys Rev Lett* 42:1058–1061. <https://doi.org/10.1103/PhysRevLett.42.1058>
- Cowley SWH (1982) The causes of convection in the Earth's magnetosphere: a review of developments during IMS. *Rev Geophys* 20:531–565
- Cowley SWH, Lockwood M (1992) Excitation and decay of solar-wind driven flows in the magnetosphere-ionosphere system. *Ann Geophys* 10:103–115
- Crooker NU (1979) Dayside merging and cusp geometry. *J Geophys Res* 84:951–959
- Daly PW, Sanderson TR, Wenzel K-P (1984) Survey of energetic ($E > 35$ keV) ion anisotropies in the deep geomagnetic tail. *J Geophys Res* 89:10733–10739. <https://doi.org/10.1029/JA089iA12p10733>
- DeJong AD, Clauer CR (2005) Polar UVI images to study steady magnetospheric convection events: initial results. *Geophys Res Lett* 32:L24101. <https://doi.org/10.1029/2005GL024498>
- DeJong AD, Cai X, Clauer RC, Spann JF (2007) Aurora and open magnetic flux during isolated substorms, sawteeth, and SMC events. *Ann Geophys* 25:1865–1876. <https://doi.org/10.5194/angeo-25-1865-2007>
- Dubyagin SV, Sergeev VA, Apatenkov SV, Angelopoulos V, Nakamura R, McFadden J, Larson D, Bonnell J (2010) Pressure and entropy changes in the flow-braking region during magnetic fielddepolarizationn. *J Geophys Res* 115:A10225. <https://doi.org/10.1029/2010JA015625>
- Dungey JW (1950) Some researches in cosmic magnetism. PhD Thesis, Cambridge University
- Dungey JW (1958) *Cosmic electrodynamics*. Cambridge University Press, Cambridge
- Dungey JW (1961) Interplanetary magnetic field and the auroral zones. *Phys Rev Lett* 6:47–48
- Dungey JW (1962) The interplanetary field and auroral theory. *J Phys Soc Jpn* 17(suppl. a–ii):15–19
- Dungey JW (1963) The structure of the ionosphere, or adventures in velocity space. In: DeWitt C, Hiebolt J, Lebeau A (eds) *Geophysics: the Earth's environment*. Gordon and Breach, New York, pp 526–536
- Dunlop MW, Zhang Q-H, Bogdanova YV, Trattner KJ, Pu Z, Hasegawa H, Berchem J, Taylor MGGT, Volwerk M, Eastwood JP, Lavraud B, Shen C, Shi J-K, Wang J, Constantinescu D, Fazakerley AN, Frey H, Sibeck D, Escoubet P, Wild JA, Liu ZX, Carr C (2011) Magnetopause reconnection across wide local time. *Ann Geophys* 29:1683–1697. <https://doi.org/10.5194/angeo-29-1683-2011>
- Eggington JWB, Eastwood JP, Mejnertsen L, Desai RT, Chittenden JP (2020) Dipole tilt effect on magnetopause reconnection and the steady-state magnetosphere-ionosphere system: global MHD simulations. *J Geophys Res Space Phys* 125:e2019JA027510. <https://doi.org/10.1029/2019JA027510>

- El-Alaoui M, Ashour-Abdalla M, Walker R, Peroomian V, Richard R, Angelopoulos V, Runov A (2009) Substorm evolution as revealed by themissatellites and a global MHD simulation. *J Geophys Res* 114:A08221. <https://doi.org/10.1029/2009JA014133>
- Erickson GM, Wolf RA (1980) Is steady convection possible in the Earth's magnetotail? *Geophys Res Lett* 7:897–900
- Eriksson S et al (2016) Magnetospheric Multiscale observations of magnetic reconnection associated with Kelvin-Helmholtz waves. *Geophys Res Lett* 43. <https://doi.org/10.1002/2016GL068783>
- Frank L (1971) Plasma in the Earth's polar magnetosphere. *J Geophys Res* 76:5202
- Frey HU, Mende SB, Fuselier SA, Immel TJ, Ostgaard N (2003) Proton aurora in the cusp during southward IMF. *J Geophys Res* 108(A7):1277. <https://doi.org/10.1029/2003JA009861>
- Fu H, Grigorenko EE, Gabrielse C, Liu C, Lu S, Hwang KJ, Zhou X, Wang Z, Chen F (2020) Magnetotail-polarization fronts and particle acceleration: a review. *Sci China Earth Sci* 63:235–256. <https://doi.org/10.1007/s11430-019-9551-y>
- Funsten HO, Allegrini F, Bochsler P, Dunn G, Ellis S, Everett D, Fagan MJ, Fuselier SA, Granoff M, Gruntman M, Guthrie AA, Hanley J, Harper RW, Heirtzler D, Janzen P, Kihara KH, King B, Kucharek H, Manzo MP, Maple M, Mashburn K, McComas DJ, Moebius E, Nolin J, Piazza D, Pope S, Reisenfeld DB, Rodriguez B, Roelof EC, Saul L, Turco S, Walek P, Weidner S, Wurz P, Zaffke S (2009) The Interstellar Boundary Explorer High Energy (IBEX-Hi) neutral atom imager. *Space Sci Rev* 146(1):75. <https://doi.org/10.1007/s11214-009-9495-8>
- Fuselier SA, Klumpp DM, Peterson WK, Shelley EG (1989) Direct injection of ionospheric O⁺ into the dayside low latitude boundary layer. *Geophys Res Lett* 16(10):1121–1124. <https://doi.org/10.1029/GL016i010p01121>
- Fuselier SA, Anderson BJ, Onsager TG (1995) Particle signatures of magnetic topology at the magnetopause: AMPTE/CCE observations. *J Geophys Res* 100:11805–11822
- Fuselier SA, Shelley EG, Peterson WK, Lennartsson OW, Collin HL, Drake JF, Ghielmetti AG, Balsiger H, Burch JL, Johnstone A, Rosenbauer H, Steinberg JT (1997) Bifurcated cusp ion signatures: evidence for quasi-steady re-reconnection? *Geophys Res Lett* 24:1471–1474
- Fuselier SA, Frey HU, Trattner KJ, Mende SB, Burch JL (2002) Cusp aurora dependence on interplanetary magnetic field B_z. *J Geophys Res* 107. <https://doi.org/10.1029/2001JA900165>
- Fuselier SA, Mende SB, Moore TE, Frey HU, Petrinec SM, Claffin ES, Collier MR (2003) Cusp dynamics and ionospheric outflow. *Space Sci Rev* 109:285–312. <https://doi.org/10.1023/B:SPAC.0000007522.71147.b3>
- Fuselier SA, Bochsler P, Chornay D, Clark G, Crew GB, Dunn G, Ellis S, Friedmann T, Funsten HO, Ghielmetti AG, Googins J, Granoff MS, Hamilton JW, Hanley J, Heirtzler D, Hertzberg E, Isaac D, King B, Knauss U, Kucharek H, Kurdirka F, Livi S, Lobell J, Longworth S, Mashburn K, McComas DJ, Möbius E, Moore AS, Moore TE, Nemanich RJ, Nolin J, O'Neal M, Piazza D, Peterson L, Pope SE, Rosmarynowski P, Saul LA, Scheer JA, Scherrer JR, Schlemm C, Schwadron NA, Tillier C, Turco S, Tyler J, Vosbury M, Wieser M, Wurz P, Zaffke S (2009) The IBEX-Lo sensor. *Space Sci Rev* 146(1):117. <https://doi.org/10.1007/s11214-009-9495-8>
- Fuselier SA, Trattner KJ, Petrinec SM, Lavraud B (2012) Dayside magnetic topology at the Earth's magnetopause for northward IMF. *J Geophys Res* 117:A08235. <https://doi.org/10.1029/2012JA017852>
- Fuselier SA, Petrinec SM, Trattner KJ, Lavraud B (2014) Magnetic field topology for northward IMF reconnection: Ion observations. *J Geophys Res* 119. <https://doi.org/10.1002/2014JA020351>
- Fuselier SA, Lewis WS, Schiff C et al (2016) Magnetospheric multiscale science mission profile and operations. *Space Sci Rev* 199:77–103. <https://doi.org/10.1007/s11214-014-0087-x>
- Fuselier SA et al (2017) Large-scale characteristics of reconnection diffusion regions and associated magnetopause crossings observed by MMS. *J Geophys Res* 122:5466–5486. <https://doi.org/10.1002/2017JA024024>
- Fuselier SA, Petrinec SM, Trattner KJ, Broll J, Burch JL, Giles BL, Strangeway RM, Russell CT, Lavraud B, Øieroset M, Torbert RB, Farrugia CJ, Vines SK, Gomez RG, Mukherjee J, Cassak PA (2018) Observational evidence of large-scale multiple reconnection at the Earth's dayside magnetopause. *J Geophys Res* 123:8407–8421. <https://doi.org/10.1029/2018JA025681>
- Fuselier SA, Trattner KJ, Petrinec SM, Denton MH, Toledo-Redondo S, André M et al (2019a) Mass loading the Earth's dayside magnetopause boundary layer and its effect on magnetic reconnection. *Geophys Res Lett* 46:6204–6213. <https://doi.org/10.1029/2019GL082384>
- Fuselier SA, Trattner KJ, Petrinec SM, Pritchard KR, Burch JL, Cassak PA et al (2019b) Stationarity of the reconnection X-line at Earth's magnetopause for southward IMF. *J Geophys Res* 124:8524–8534. <https://doi.org/10.1029/2019JA027143>
- Fuselier SA, Webster JM, Trattner KJ, Petrinec SM, Genestreti KJ, Pritchard KR et al (2021) Reconnection x-line orientations at the Earth's magnetopause. *J Geophys Res* 126. <https://doi.org/10.1029/2021JA029789>

- Fuselier SA, Kletzing CA, Petrinec SM, Trattner KJ, George D, Bounds SR, Sawyer RP, Bonnell JW, Burch JL, Giles BL, Strangeway RJ (2022) Multiple reconnection X-lines at the magnetopause and overlapping cusp ion injections. *J Geophys Res* 127:e2022JA030354. <https://doi.org/10.1029/2022JA030354>
- Galeev AA, Sudan RN (1984) Basic plasma physics: selected chapters, handbook of plasma physics, vol 1. North-Holland, Amsterdam, p 305
- Gjerloev JW (2012) The supermag data processing technique. *J Geophys Res* 117(A9). <https://doi.org/10.1029/2012JA017683>
- Glocer A, Welling D, Chappell CR, Toth G, Fok MC, Komar C et al (2020) A case study on the origin of near-Earth plasma. *J Geophys Res* 125:e2020JA028205. <https://doi.org/10.1029/2020JA028205>
- Gomez RG, Vines SK, Fuselier SA, Cassak PA, Strangeway RJ, Petrinec SM, Burch JL, Trattner KJ, Russell CT, Torbert RB, Pollock C, Young DT, Lewis WS, Mukherjee J (2016) Stable reconnection at the dusk flank magnetopause. *Geophys Res Lett* 43:9374–9382. <https://doi.org/10.1002/2016GL069692>
- Gonzalez WD, Mozer FS (1974) A quantitative model for the potential resulting from reconnection with an arbitrary interplanetary magnetic field. *J Geophys Res* 79:4186–4194
- Gonzalez W, Parker E (2016) Magnetic reconnection: concepts and applications. Astrophysics and space science library, vol 427. Springer, Cham. <https://doi.org/10.1007/978-3-319-26432-5>
- Gordeev E, Sergeev V, Merkin V, Kuznetsova M (2017) On the origin of plasma sheet reconfiguration during the substorm growth phase. *Geophys Res Lett* 44:8696–8702. <https://doi.org/10.1002/2017GL074539>
- Gosling JT, Thomsen MF, Bame SJ, Onsager TG, Russell CT (1990) Electron edge of the low latitude boundary layer during accelerated flow events. *Geophys Res Lett* 17:1833–1836
- Griffiths ST, Petrinec SM, Trattner KJ, Fuselier SA, Burch JL, Phan TD, Angelopoulos V (2011) A probability assessment of encountering dayside magnetopause diffusion regions. *J Geophys Res* 116:A02214. <https://doi.org/10.1029/2010JA015316>
- Grocott A, Cowley SWH, Sigwarth JB (2003) Ionospheric flows and magnetic disturbance during extended intervals of northward but by-dominated IMF. *Ann Geophys* 21:509–538. <https://doi.org/10.5194/angeo-21-509-2003>
- Grocott A, Yeoman TK, Milan SE, Amm O, Frey HU, Juusola L, Nakamura R, Owen CJ, Rème H, Takada T (2007) Multi-scale observations of magnetotail flux transport during IMF-northward non-substorm intervals. *Ann Geophys* 25:1709–1720
- Hardy DA, Reiff PH, Burke WJ (1979) Response of magnetotail plasma at lunar distance to changes in the interplanetary magnetic field, the solar wind plasma, and substorm activity. *J Geophys Res* 84:1382–1390. <https://doi.org/10.1029/g1005i005p00391>
- Hasegawa H et al (2010) Evidence for a flux transfer event generated by multiple X-line reconnection at the magnetopause. *Geophys Res Lett* 37:L16101. <https://doi.org/10.1029/2010GL044219>
- Heelis RA (1984) The effects of interplanetary magnetic field orientation on dayside high-latitude ionospheric convection. *J Geophys Res* 89:2873–2880. <https://doi.org/10.1029/JA089iA05p02873>
- Heikkila WJ, Winningham JD (1971) Penetration of magnetosheath plasma to low altitudes through the dayside magnetospheric cusps. *J Geophys Res* 76:883–891. <https://doi.org/10.1029/JA076i004p00883>
- Henderson M (2004) The May 2–3, 1986 CDAW-9C interval: a sawtooth event. *Geophys Res Lett* 31(11):L11804. <https://doi.org/10.1029/2004gl019941>
- Henderson MG, Reeves GD, Skoug R, Thomsen MT, Denton MH, Mende SB, Immel TJ, Brandt PC, Singer HJ (2006) Magnetospheric and auroral activity during the 18 April 2002 sawtooth event. *J Geophys Res* 111:A01S90. <https://doi.org/10.1029/2005JA011111>
- Hesse M, Birn J (1994) MHD modeling of magnetotail instability for localized resistivity. *J Geophys Res* 99(A5):8565–8576. <https://doi.org/10.1029/94JA00441>
- Hesse M, Aunai N, Zenitani S, Kuznetsova M, Birn J (2013) Aspects of collisionless magnetic reconnection in asymmetric systems. *Phys Plasmas* 20(6):061210. <https://doi.org/10.1063/1.4811467>
- Hill TW, Reiff PH (1977) Evidence of magnetospheric cusp proton acceleration by magnetic merging at the dayside magnetopause. *J Geophys Res* 82:3623–3628. <https://doi.org/10.1029/JA082i025p03623>
- Hones EW Jr (1977) Substorm processes in the magnetotail: comments on “On hot tenuous plasmas, fireballs, and boundary layers in the Earth’s magnetotail” by Frank et al. *J Geophys Res* 82:5633
- Hones EW Jr, Birn J, Baker DN et al (1984) Detailed examination of a plasmoid in the distant magnetotail with ISEE 3. *Geophys Res Lett* 11(10):1046–1049. <https://doi.org/10.1029/GL011i010p01046>
- Hsieh M-S, Otto A (2014) The influence of magnetic flux depletion on the magnetotail and auroral morphology during the substorm growth phase. *J Geophys Res* 119(5):3430–3443. <https://doi.org/10.1002/2013JA019459>
- Hsieh M-S, Otto A (2015) Thin current sheet formation in response to the loading and the depletion of magnetic flux during the substorm growth phase. *J Geophys Res* 120(6):4264–4278. <https://doi.org/10.1002/2014JA020925>
- Huang CY, Frank LA, Rostoker G, Fennell J, Mitchell DG (1992) Nonadiabatic heating of the central plasma sheet at substorm onset. *J Geophys Res* 82:1481–1495

- Huang C-S, Reeves GD, Borovsky JE, Skoug RM, Pu ZY, Le G (2003) Periodic magnetospheric substorms and their relationship with solar wind variations. *J Geophys Res* 108(A6):1255. <https://doi.org/10.1029/2002JA009704>
- Hughes WJ, Sibeck DG (1987) On the 3-dimensional structure of plasmoids. *Geophys Res Lett* 14(6):636–639. <https://doi.org/10.1029/GL014i006p00636>
- Hwang KJ, Nakamura R, Eastwood JP et al (2023) Cross-scale processes of magnetic reconnection. *Space Sci Rev* 219:71. <https://doi.org/10.1007/s11214-023-01010-9>
- Kamide Y, Perrault PD, Akasofu S-I, Winningham JD (1977) Dependence of substorm occurrence probability on the interplanetary magnetic field and on the size of the auroral oval. *J Geophys Res* 82:5521
- Keiling A, Angelopoulos V, Runov A, Weygand J, Apatenkov SV, Mende S et al (2009) Substorm current wedge driven by plasma flow vortices: THEMIS observations. *J Geophys Res* 114. <https://doi.org/10.1029/2009JA014114>
- Keiling A, Ramos C, Vu N, Angelopoulos V, Nosé M (2022) Statistical properties and proposed source mechanism of recurrent substorm activity with one-hour periodicity. *J Geophys Res* 127:e2021JA030064. <https://doi.org/10.1029/2021JA030064>
- Kepko L, McPherron R, Amm O, Apatenkov S, Baumjohann W, Birn J et al (2015) Substorm current wedge revisited. *Space Sci Rev* 190:1–46. <https://doi.org/10.1007/s11214-014-0124-9>
- Khotyaintsev YV, Cully CM, Vaivads A, André M, Owen CJ (2011) Plasma jet braking: energy dissipation and nonadiabatic electrons. *Phys Rev Lett* 106(16):165001. <https://doi.org/10.1103/PhysRevLett.106.165001>
- Khrabrov AV, Sonnerup BUÖ (1998) Orientation and motion of current layers: minimization of the Faraday residue. *Geophys Res Lett* 25:2373–2376. <https://doi.org/10.1029/98GL51784>
- Kiehas SA, Angelopoulos V, Runov A, Hietala H, Korovinskiy D (2018) Magnetotail fast flow occurrence rate and dawn-dusk asymmetry at XGSM $\sim 60R_E$. *J Geophys Res* 123. <https://doi.org/10.1002/2017JA024776>
- Kissinger J, McPherron RL, Hsu T-S, Angelopoulos V (2012) Diversion of plasma due to high pressure in the inner magnetosphere during steady magnetospheric convection. *J Geophys Res* 117:A05206. <https://doi.org/10.1029/2012JA017579>
- Kistler LM (2020) Ionospheric and solar wind contributions to the storm-time near-Earth plasma sheet. *Geophys Res Lett* 47:e2020GL090235. <https://doi.org/10.1029/2020GL090235>
- Kistler LM, Ipavich FM, Hamilton DC, Gloeckler G, Wilken B, Kremser G, Stüdemann W (1989) Energy spectra of the major ion species in the ring current during geomagnetic storms. *J Geophys Res* 94:3579–3599
- Kistler LM, Mouikis CG, Asamura K, Yokota S, Kasahara S, Miyoshi Y et al (2019) Cusp and nightside auroral sources of O^+ in the plasma sheet. *J Geophys Res* 124. <https://doi.org/10.1029/2019JA027061>
- Kivelson MG, Spence HE (1988) On the possibility of quasi-static convection in the quiet magnetotail. *Geophys Res Lett* 15:1541–1544
- Kronberg EA, Daly PW, Grigorenko EE, Smirnov AG, Klecker B, Malykhin AY (2021) Energetic charge particles in the terrestrial magnetosphere: cluster/RAPID results. *J Geophys Res* 126:E2021JA029273. <https://doi.org/10.1029/2021JA029273>
- Kuznetsova MM, Hesse M, Rasta'tter L, Taktakishvili A, Toth G, De Zeeuw DL, Ridley A, Gombosi TI (2007) Multiscale modeling of magnetospheric reconnection. *J Geophys Res* 112:A10210. <https://doi.org/10.1029/2007JA012316>
- Lavaud B, Borovsky JE (2008) Altered solar wind-magnetosphere interaction at low Mach numbers: Coronal mass ejections. *J Geophys Res* 113. <https://doi.org/10.1029/2008JA013192>
- Lavraud B, Trattner KJ (2021) The polar cusps of the Earth's magnetosphere. In: Moretti R (ed) *Magnetospheres in the Solar System, 10th anniversary of the AGU*. Geophysical monograph series, vol 2, pp 163–176. <https://doi.org/10.1002/9781119815624.ch11>
- Lavraud B, Thomsen MF, Taylor MGGT, Wang YL, Phan TD, Schwartz SJ et al (2005) Characteristics of the magnetosheath electron boundary layer under northward IMF: implications for high-latitude reconnection. *J Geophys Res* 110:A06209. <https://doi.org/10.1029/2004JA010808>
- Lavraud B, Thomsen MF, Lefebvre B, Schwartz SJ, Seki K, Phan TD et al (2006) Evidence for newly closed magnetosheath field lines at the dayside magnetopause under northward IMF. *J Geophys Res* 111(A5):A05211. <https://doi.org/10.1029/2005JA011266>
- Lavraud B, Jacquy C, Achilli T, Fuselier SA, Grigorenko E, Phan TD et al (2018) Concomitant double ion and electron populations in the Earth's magnetopause boundary layers from double reconnection with lobe and closed field lines. *J Geophys Res* 123:5407–5419. <https://doi.org/10.1029/2017JA025152>
- Lee LC, Fu ZF (1986) Multiple X line reconnection. I. A criterion for the transition from a single X line to multiple X line reconnection. *J Geophys Res* 91:6807
- Lee D-Y, Choi K-C, Ohtani S, Lee JH, Kim KC, Park KS, Kim K-H (2010) Can intense substorms occur under northward IMF conditions? *J Geophys Res* 115:A01211. <https://doi.org/10.1029/2009JA014480>

- Li S-S, Angelopoulos V, Runov A, Kiehas SA (2014) Azimuthal extent and properties of midtail plasmoids from two-point ARTEMIS observations at the Earth-Moon Lagrange points. *J Geophys Res* 119:1781–1796. <https://doi.org/10.1002/2013JA019292>
- Li W, André M, Khotyaintsev YV, Vaivads A et al (2016) Kinetic evidence of magnetic reconnection due to Kelvin-Helmholtz waves. *Geophys Res Lett* 43:5635–5643. <https://doi.org/10.1002/2016GL069192>
- Liu J, Angelopoulos V, Runov A, Zhou X-Z (2013a) On the current sheets surrounding dipolarizing flux bundles in the magnetotail: the case for wedgelets. *J Geophys Res* 118. <https://doi.org/10.1002/jgra.50092>
- Liu J, Angelopoulos V, Chu X, Zhou XZ, Yue C (2015) Substorm current wedge composition by wedgelets. *Geophys Res Lett* 42:1669–1676. <https://doi.org/10.1002/2015GL063289>
- Lockwood M (1995) Overlapping cusp ion injections: an explanation invoking magnetopause reconnection. *Geophys Res Lett* 22:1141
- Lockwood M (1997) Energy and pitch-angle dispersions of LLBL/cusp ions seen at middle altitudes: predictions by the open magnetosphere model. *Ann Geophys* 15:1501–1514. <https://doi.org/10.1007/s00585-997-1501-4>
- Lockwood M, Bentley SN, Owens MJ, Barnard LA et al (2019) The development of a space climatology: 1. Solar wind magnetosphere coupling as a function of timescale and the effect of data gaps. *Space Weather* 17:133–156. <https://doi.org/10.1029/2018SW001856>
- Luhmann JR, Walker RJ, Russell CT, Crooker NU, Spreiter JR, Stahara SS (1984) Patterns of potential magnetic field merging sites on the dayside magnetopause. *J Geophys Res* 89:1739–1742
- McComas DJ, Allegrini F, Bochsler P, Bzowski M, Collier M, Fahr H, Fichtner H, Frisch P, Funsten HO, Fuselier S, Gloeckler G, Gruntman M, Izmodenov V, Knappenberger P, Lee M, Livi S, Mitchell D, Möbius E, Moore T, Pope S, Reisenfeld D, Roelof E, Scherrer J, Schwadron N, Tyler R, Wieser M, Witte M, Wurz P, Zank G (2009) IBEX – interstellar boundary explorer. *Space Sci Rev* 146(1):11. <https://doi.org/10.1007/s11214-009-9495-8>
- McPherron RL (1972) Substorm related changes in the geomagnetic tail: the growth phase. *Planet Space Sci* 20:1521–1539
- McPherron RL, Chu X (2018) The midlatitude positive bay index and the statistics of substorm occurrence. *J Geophys Res* 123:2831–2850. <https://doi.org/10.1002/2017JA024766>
- McPherron RL, Russell CT, Aubry MA (1973) Satellite studies of magnetospheric substorms on August 15 1968: 9. Phenomenological model for substorms. *J Geophys Res* 78:3131
- McPherron RL, Nishida A, Russell CT (1987) Is near-Earth current sheet thinning the cause of auroral substorm onset? In: Kamide Y, Wolf RA (eds) Quantitative modeling of the magnetosphere-ionosphere coupling processes, p 252. Kyoto Sangyo University, Kyoto
- Merkin VG, Panov EV, Sorathia KA, Ukhorskiy AY (2019) Contribution of bursty bulk flows to the global dipolarization of the magnetotail during an isolated substorm. *J Geophys Res* 124
- Michotte de Welle B, Aunai N, Nguyen G, Lavraud B, Génot V, Jeandet A, Smets R (2022) Global three-dimensional draping of magnetic field lines in Earth's magnetosheath from in-situ spacecraft measurements. *J Geophys Res Space Phys* 127:e2022JA030996. <https://doi.org/10.1029/2022JA030996>
- Milan SE, Hubert B, Grocott A (2005) Formation and motion of a transpolar arc in response to dayside and nightside reconnection. *J Geophys Res* 110. <https://doi.org/10.1029/2004JA010835>
- Milan SE, Grocott A, Forsyth C, Imber SM, Boakes PD, Hubert B (2009) A superposed epoch analysis of auroral evolution during substorm growth, onset and recovery: open magnetic flux control of substorm intensity. *Ann Geophys* 27:659–668. <https://doi.org/10.5194/angeo-27-659-2009>
- Milan SE, Clausen LBN, Coxon JC et al (2017) Overview of solar wind–magnetosphere–ionosphere–atmosphere coupling and the generation of magnetospheric currents. *Space Sci Rev* 206:547–573. <https://doi.org/10.1007/s11214-017-0333-0>
- Miyashita Y et al (2005) Plasmoids observed in the near-Earth magnetotail at $X \sim -7R_E$. *J Geophys Res* 110:A12214. <https://doi.org/10.1029/2005JA011263>
- Moldwin MB, Hughes WJ (1992) On the formation and evolution of plasmoids: a survey of ISEE 3 geotail data. *J Geophys Res* 97(A12):19259–19282. <https://doi.org/10.1029/92JA01598>
- Moore TE, Fok M-C, Chandler MO (2002) The dayside reconnection X line. *J Geophys Res* 107:1332–1338. <https://doi.org/10.1029/2002JA009381>
- Moore TE, Fok M-C, Delcort DC, Slinker SP, Fedder JA (2008) Plasma plume circulation and impact in an MHD substorm. *J Geophys Res* 113:A06219. <https://doi.org/10.1029/2008JA013050>
- Nagai T (2021) Magnetic reconnection in the near-Earth magnetotail. In: Maggiolo R, André N, Hasegawa H, Welling DT (eds) Space physics and aeronomy collection volume 2: magnetospheres in the Solar System, 1st edn. Geophysical monograph, vol 259. Am. Geophys. Union, Washington. <https://doi.org/10.1002/9781119815624.ch4>
- Nagai T, Machida S (1998) Magnetic reconnection in the near-Earth magnetotail. In: Nishida A, Baker DN, Cowley SWH (eds) New perspectives on the Earth's magnetotail. Geophysical monograph, vol 105. Am. Geophys. Union, Washington, pp 211–224

- Nagai T, Fujimoto M, Saito Y, Machida S, Terasawa T, Nakamura R, Yamamoto T, Mukai T, Nishida A, Kokubun S (1998) Structure and dynamics of magnetic reconnection for substorm onsets with Geotail observations. *J Geophys Res* 103:4419–4440
- Nagai T, Fujimoto M, Nakamura R, Baumjohann W, Ieda A, Shinohara I, Machida S, Saito Y, Mukai T (2005) Solar wind control of the radial distance of the magnetic reconnection site in the magnetotail. *J Geophys Res* 110. <https://doi.org/10.1029/2005JA011207>
- Nakamura R, Baker DN, Yamamoto T, Belian RD, Bering EA III, Benbrook JR, Theall JR (1994) Particle and field signatures during pseudobreakup and major expansion onset. *J Geophys Res* 99:207–221
- Nakamura R, Baumjohann W, Brittnacher M, Sergeev VA, Kubyskhina M, Mukai T, Liou K (2001a) Flow bursts and auroral activations: onset timing and foot point location. *J Geophys Res* 106:10777–10789
- Nakamura R, Baumjohann W, Schödel R, Brittnacher M, Sergeev VA, Kubyskhina M, Liou K (2001b) Earthward flow bursts, auroral streamers, and small expansions. *J Geophys Res* 106:10791–10802
- Nakamura R, Baumjohann W, Mouikis C, Kistler LM, Runov A, Volwerk M, Asano Y, Vörös Z, Zhang TL, Klecker B, Réme H, Balogh A (2004) Spatial scale of high-speed flows in the plasma sheet observed by Cluster. *Geophys Res Lett* 31:L09804. <https://doi.org/10.1029/2004GL019558>
- Nakamura R et al (2011) Flux transport, dipolarization, and current sheet evolution during a double-onset substorm. *J Geophys Res* 116:A00I36. <https://doi.org/10.1029/2010JA0156865>
- Nishida A, Scholer M, Terasawa T, Bame SJ, Gloeckler G, Smith EJ, Zwickl RD (1986) Quasi-stagnant plasmoid in the middle tail: a new preexpansion phase phenomenon. *J Geophys Res* 91:4245–4255. <https://doi.org/10.1029/JA091iA04p04245>
- Nykyri K, Otto A (2001) Plasma transport at the magnetospheric boundary due to reconnection in Kelvin-Helmholtz vortices. *Geophys Res Lett* 28:3565–3568. <https://doi.org/10.1029/2001GL013239>
- Nykyri K, Otto A, Lavraud B, Mouikis C, Kistler L, Balogh A, Réme H (2006) Cluster observations of reconnection due to the Kelvin-Helmholtz instability at the dawnside magnetospheric flank. *Ann Geophys* 24:2619–2643
- Nykyri K, Ma X, Johnson J (2021) Cross-scale energy transport in space plasmas: applications to the magnetopause boundary. In: Maggiolo R, André N, Hasegawa H, Welling DT (eds) Space physics and aeronomy collection volume 2: magnetospheres in the Solar System, 1st edn. Geophysical monograph, vol 259. Am. Geophys. Union, Washington. <https://doi.org/10.1002/9781119815624.ch6>
- Øieroset M, Phan TD, Lin RP, Sonnerup BUÖ (2000) *J Geophys Res* 105(25):247–250
- Øieroset M, Phan TD, Fujimoto M, Lin RP, Lepping RP (2001) In situ detection of collisionless reconnection in the Earth's magnetotail. *Nature* 412:26
- Øieroset M, Phan TD, Angelopoulos V, Eastwood JP, McFadden J, Larson D, Carlson CW, Glassmeier K-H, Fujimoto M, Raeder J (2008) THEMIS multi-spacecraft observations of magnetosheath plasma penetration deep into the dayside low-latitude magnetosphere for northward and strong B_Y IMF. *Geophys Res Lett* 35:L17S11. <https://doi.org/10.1029/2008GL033661>
- Oka M, Phan TD, Øieroset M et al (2022) Electron energization and thermal to non-thermal energy partition during Earth's magnetotail reconnection. *Phys Plasmas* 29(5):052904. <https://doi.org/10.1063/5.0085647>
- Oka M, Birn J, Egedal J et al (2023) Particle acceleration by magnetic reconnection in geospace. *Space Sci Rev* 219:75. <https://doi.org/10.1007/s11214-023-01011-8>
- Onsager TG, Chang S-W, Perez JD, Austin JB, Jano LX (1995) Low-altitude observations and modeling of quasi-steady magnetopause reconnection. *J Geophys Res* 100:11831–11843
- Otto A, Fairfield DH (2000) Kelvin-Helmholtz instability at the magnetotail boundary: MHD simulation and comparison with Geotail observations. *J Geophys Res* 105:21175–21190
- Ouellette JE, Brambles OJ, Lyon JG, Lotko W, Rogers BN (2013) Properties of outflow-driven sawtooth substorms. *J Geophys Res* 118:3223–3232. <https://doi.org/10.1002/jgra.50309>
- Park KS (2021) Global MHD simulation of the weak southward IMF condition for different time resolutions. *Front Astron Space Sci* 8:758241. <https://doi.org/10.3389/fspas.2021.758241>
- Peng Z, Wang C, Yang YF, Li H, Hu YQ, Du J (2013) Substorms under northward interplanetary magnetic field: statistical study. *J Geophys Res* 118:364–374. <https://doi.org/10.1029/2012JA018065>
- Peterson WK et al (1998) Simultaneous observations of solar wind plasma entry from FAST and POLAR. *Geophys Res Lett* 25:2081
- Petrinec SM, Fuselier SA (2003) On continuous versus discontinuous neutral lines at the dayside magnetopause for southward interplanetary magnetic field. *Geophys Res Lett* 30(10):1519. <https://doi.org/10.1029/2002GL016565>
- Petrinec SM, Dayeh MA, Funsten HO, Fuselier SA, Heirtzler D, Janzen P, Kucharek H, McComas DJ, Möbius E, Moore TE, Reisenfeld DB, Schwadron N, Trattner KJ, Wurz P (2011) Neutral atom imaging of the magnetospheric cusps. *J Geophys Res* 116:A07203. <https://doi.org/10.1029/2010JA016357>
- Petrinec SM, Burch JL, Fuselier SA, Gomez RG, Lewis W, Trattner KJ, Ergun R, Mauk B, Pollock CJ, Schiff C, Strangeway RJ, Russell CT, Phan T-D, Young D (2016) Comparison of Magnetospheric Multiscale

- ion jet signatures with predicted reconnection site locations at the magnetopause. *Geophys Res Lett* 43. <https://doi.org/10.1002/2016GL069626>
- Petrinec SM, Burch JL, Fuselier SA, Trattner KJ, Giles BL, Strangeway RJ (2022) On the occurrence of magnetic reconnection along the terrestrial magnetopause, using Magnetospheric Multiscale (MMS) observations in proximity to the reconnection site. *J Geophys Res* 127. <https://doi.org/10.1029/2021JA029669>
- Petrukovich AA, Baumjohann W, Nakamura R, Mukai T, Troshichev OA (2000) Small substorms: solar wind input and magnetotail dynamics. *J Geophys Res* 105:21109–21118. <https://doi.org/10.1029/2000JA900057>
- Petschek HE (1964) Magnetic field annihilation. In: Hess WN (ed) AAS NASA Symp. Phys. Solar Flares. NASA, vol SP-50, pp 425–437
- Phan TD, Kistler LM, Klecker B, Haerendel G, Paschmann G, Sonnerup BUÖ, Baumjohann W, Bavassano-Cattaneo MB, Carlson CW, DiLellis AM, Fornacon K-H, Frank LA, Fujimoto M, Georgescu E, Kokubun S, Moebius E, Mukai T, Oieroset M, Paterson WR, Rème H (2000) Extended magnetic reconnection at the Earth's magnetopause from detection of bi-directional jets. *Nature* 404:848–850
- Phan T, Frey HU, Frey S, Peticolas L, Fuselier S, Carlson C, Reme H, Bosqued J-M, Balogh A, Dunlop M, Kistler L, Mouikis C, Dandouras I, Sauvaud J-A, Mende S, McFadden J, Parks G, Moebius E, Klecker B, Paschmann G, Fujimoto M, Petrinec S, Maruccci MF, Korth A, Lundin R (2003) Simultaneous Cluster and IMAGE observations of cusp reconnection and auroral proton spot for northward IMF. *Geophys Res Lett* 30(10):1509. <https://doi.org/10.1029/2003GL016885>
- Phan TD, Hasegawa H, Fujimoto M, Oieroset M, Mukai T, Lin RP, Paterson W (2006) Simultaneous geotail and wind observations of reconnection at the subsolar and tail flank magnetopause. *Geophys Res Lett* 33:9. <https://doi.org/10.1029/2006GL025756>
- Phan TD, Shay MA, Gosling JT et al (2013) Electron bulk heating in magnetic reconnection at Earth's magnetopause: dependence on the inflow Alfvén speed and magnetic shear. *Geophys Res Lett* 40(17):4475–4480. <https://doi.org/10.1002/grl.50917>
- Pi G, Shue J, Chao J, Němeček Z, Šafránková J, Lin C (2014) A reexamination of long-duration radial IMF events. *J Geophys Res* 119(9):7005–7011. <https://doi.org/10.1002/2014ja019993>
- Pontius D, Wolf RA (1990) Transient flux tubes in the terrestrial magnetosphere. *Geophys Res Lett* 17:49
- Pulkkinen TI, Baker DN, Mitchell DG, McPherron RL, Huang CY, Frank LA (1992) Global and local current sheet thickness estimates during the late growth phase. In: Proceedings of the International Conference on Substorms (ICS-1). European Space Agency, Paris, p 131
- Raeder J (2003) Global magnetohydrodynamics – a tutorial. In: Büchner J, Scholer M, Dum CT (eds) Space plasma simulation. Lecture Notes in Physics, vol 615. Springer, Berlin, Heidelberg, pp 212–246. https://doi.org/10.1007/3-540-36530-3_11
- Raeder J (2022) Global simulations. In: Maggiolo R, André N, Hasegawa H, Welling DT (eds) Space physics and aeronomy collection volume 2: magnetospheres in the Solar System, 1st edn. Geophysical monograph, vol 259. Am. Geophys Union, Washington. <https://doi.org/10.1002/9781119815624>
- Raeder J, Berchem J, Ashour-Abdalla M (1996) The importance of small scale processes in global MHD simulations: some numerical experiments. In: Chang T, Jasperse JR (eds) The physics of space plasmas, vol 14. MIT Center for Theoretical Geo/Cosmo Plasma Physics, Cambridge, MA, p 403
- Reiff PH, Hill TW, Burch JL (1977) Solar-wind plasma injection at the dayside magnetospheric cusp. *J Geophys Res* 82:479–491. <https://doi.org/10.1029/JA082i004p00479>
- Reiff PH, Daou AG, Sazykin SY et al (2016) Multispacecraft observations and modeling of the 22/23 June 2015 geomagnetic storm. *Geophys Res Lett* 43:7311–7318. <https://doi.org/10.1002/2016GL069154>
- Reiff PH, Marshall A, Webster J, Sazykin S, Russell CT, Rastaetter L (2018) MMS observations and CCMC modeling of field line stretching at separator lines. Fall AGU e-Lightning poster, <https://agu2018fallmeeting-agu.ipostersessions.com/default.aspx?s=B2-10-20-70-BD-2D-A2-4E-35-27-A4-FE-DC-C0-6D-dA>. <https://doi.org/10.1002/essoar.10502075.1>
- Rogers B, Zakharov L (1995) Nonlinear ω^* -stabilization of the $m = 1$ mode in tokamaks. *Phys Plasmas* 2:3420. <https://doi.org/10.1063/1.871124>
- Rogers AJ, Farrugia CJ, Torbert RB (2019) Numerical algorithm for detecting ion diffusion regions in the geomagnetic tail with applications to MMS tail season 1 May to 30 September 2017. *J Geophys Res* 124:6487–6503. <https://doi.org/10.1029/2018JA026429>
- Rogers AJ, Farrugia CJ, Torbert RB, Rogers TJ (2023) Applying magnetic curvature to MMS data to identify thin current sheets relative to tail reconnection. *J Geophys Res* 128:e2022JA030577. <https://doi.org/10.1029/2022JA030577>
- Rosenbauer H, Grünwaldt H, Montgomery MD, Paschmann G, Sckopke N (1975) Heos 2 plasma observations in the distant polar magnetosphere: the plasma mantle. *J Geophys Res* 80:2723–2737. <https://doi.org/10.1029/JA080i019p02723>


- Runov A, Angelopoulos V, Artemyev AV, Weygand JM, Lu S, Li Y, Zhang X-J (2021) Global and local processes of thin current sheet formation during substorm growth phase. *J Atmos Sol-Terr Phys* 220:105671. <https://doi.org/10.1016/j.jastp.2021.105671>
- Russell CT (1972) The configuration of the magnetosphere. In: Dyer ER (ed) *Critical problems in magnetospheric physics*. National academy of sciences, p 1
- Russell CT, Elphic RC (1978) Initial ISEE magnetometer results: magnetopause observations. *Space Sci Rev* 22:681–715. <https://doi.org/10.1007/BF00212619>
- Russell CT, Strangeway RJ, Zhao C, Anderson BJ, Baumjohann W et al (2017) Structure, force balance, and topology of Earth's magnetopause. *Science* 356:960–963
- Sanny J, McPherron RL, Russel CT, Baker DN, Pulkkinen TI, Nishida A (1994) Growth-phase thinning of the near-Earth current sheet during CDAW 6 substorm. *J Geophys Res* 99:5805–5816
- Schillings A, Gunell H, Nilsson H, De Spiegeleer A, Ebihara Y, Westerberg LG, Yamauchi M, Slapak R (2020) The fate of O⁺ ions observed in the plasma mantle: particle tracing modelling and cluster observations. *Ann Geophys* 38:645–656. <https://doi.org/10.5194/angeo-38-645-2020>
- Schindler K, Baker DN, Birn J, Hones EW Jr, Slavin JA, Galvin AB (1989) Analysis of an extended period of earthward plasma flow at ~220 RE: CDAW-8. *J Geophys Res* 94:15177
- Schödel R, Baumjohann W, Nakamura R, Sergeev VA, Mukai T (2001) Rapid flux transport in the central plasma sheet. *J Geophys Res* 106:301–313. <https://doi.org/10.1029/2000JA900139>
- Scholer M, Otto A (1991) Magnetotail reconnection: current diversion and field-aligned currents. *Geophys Res Lett* 18:7331
- Sergeev VA, Tanskanen P, Mursula K, Korh A, Elphic RC (1990) Current sheet thickness in the near-Earth plasma sheet during substorm growth phase. *J Geophys Res* 95:3819
- Sergeev A, Pellinen RJ, Pulkkinen TI (1996) Steady magnetospheric convection: a review of recent results. *Space Sci Rev* 75:551–604. <https://doi.org/10.1007/BF00833344>
- Sergeev VA, Liou K, Meng CI, Newell PT, Brittnacher M, Parks G, Reeves GD (1999) Development of auroral streamers in association with localized impulsive injections to the inner magnetotail. *Geophys Res Lett* 26:417–420
- Sergeev V, Liou K, Newell PT, Ohtani SI, Hairston MR, Rich F (2004) Auroral streamers: characteristics of associated precipitation, convection and field-aligned currents. *Ann Geophys* 22:537–548
- Shelley EG, Sharp RD, Johnson RG (1976) He⁺⁺ and H⁺ flux measurements in the day side cusp: estimates of convection electric field. *J Geophys Res* 81:2363–2370. <https://doi.org/10.1029/JA081i013p02363>
- Shi QQ, Shen C, Pu ZY, Dunlop MW, Zong Q-G, Zhang H et al (2005) Dimensional analysis of observed structures using multipoint magnetic field measurements: application to cluster. *Geophys Res Lett* 32:L12105. <https://doi.org/10.1029/2005GL022454>
- Shukhtina MA, Dmitrieva NP, Sergeev VA (2014) On the conditions preceding sudden magnetotail magnetic flux unloading. *Geophys Res Lett* 41:1093–1099. <https://doi.org/10.1002/2014GL059290>
- Sitnov MI, Arnold H (2022) Equilibrium kinetic theory of weakly anisotropic embedded thin current sheets. *J Geophys Res* 127:e2022JA030945. <https://doi.org/10.1029/2022JA030945>
- Sitnov MI, Guzzdar PN, Swisdak M (2003) A model of the bifurcated current sheet. *Geophys Res Lett* 30(13):1712. <https://doi.org/10.1029/2003GL017218>
- Sitnov MI, Tsyganenko NA, Ukhorskiy AY, Brandt PC (2008) Dynamical data-based modeling of the storm-time geomagnetic field with enhanced spatial resolution. *J Geophys Res* 113(A7). <https://doi.org/10.1029/2007JA013003>
- Sitnov M, Birn J, Ferdousi B, Gordeev E, Khotyaintsev Y, Merkin V, Motoba T, Otto A, Panov E, Pritchett P, Pucci F, Raeder J, Runov A, Sergeev V, Velli M, Zhou X (2019a) Explosive magnetotail activity. *Space Sci Rev* 215:31. <https://doi.org/10.1007/s11214-019-0599-5>
- Sitnov MI, Stephens GK, Tsyganenko NA, Miyashita Y, Merkin VG, Motoba T, Ohtani S, Genestreti KJ (2019b) Signatures of nonideal plasma evolution during substorms obtained by mining multimission magnetometer data. *J Geophys Res* 124(11):8427–8456. <https://doi.org/10.1029/2019JA027037>
- Sitnov M, Stephens G, Motoba T, Swisdak M (2021) Data mining reconstruction of magnetotail reconnection and implications for its first-principal modeling. *Front Phys* 9. Retrieved from <https://www.frontiersin.org/articles/10.3389/fphy.2021.644884>. <https://doi.org/10.3389/fphy.2021.644884>
- Slavin JA, Lepping RP, Gjerloev J et al (2003) Geotail observations of magnetic flux ropes in the plasma sheet. *J Geophys Res* 108(A1):SMP10-1–SMP10-18. <https://doi.org/10.1029/2002JA009557>
- Sonnerup BUÖ (1974) The reconnecting magnetosphere. In: McCormac BM (ed) *Magnetospheric physics, proceedings of the advanced summer institute, Sheffield, UK, August 1973*. Astrophysics and space science library, vol 44. Reidel, Dordrecht, pp 23–33
- Sonnerup BUÖ, Cahill LJ Jr (1967) Magnetopause structure and attitude from explorer 12 observations. *J Geophys Res* 72:171. <https://doi.org/10.1029/JZ072i001p00171>
- Sorathia KA, Merkin VG et al (2020) Ballooning-Interchange Instability in the Near-Earth Plasma Sheet and Auroral Beads: Global Magnetospheric Modeling at the Limit of the MHD Approximation. *Geophys Res Lett* 47. <https://doi.org/10.1029/2020GL088227>

- Spence HE, Kivelson MG, Walker RJ, McComas DJ (1989) Magnetospheric plasma pressures in the midnight meridian – observations from 2.5 to 35 RE. *J Geophys Res* 4:5264–5272
- Stephens GK, Sitnov MI, Korth H, Tsyganenko NA, Ohtani S, Gkioulidou M, Ukhorskiy AY (2019) Global empirical picture of magnetospheric substorms inferred from multimission magnetometer data. *J Geophys Res* 124(2):1085–1110
- Stephens GK, Sitnov MI, Weigel RS, Turner DL, Tsyganenko NA, Rogers AJ et al (2023) Global structure of magnetotail reconnection revealed by mining space magnetometer data. *J Geophys Res* 128:e2022JA031066. <https://doi.org/10.1029/2022JA031066>
- Sun WJ, Slavin JA, Tian AM et al (2019) MMS study of the structure of ion-scale flux ropes in the Earth's cross-tail current sheet. *Geophys Res Lett* 46(12):6168–6177. <https://doi.org/10.1029/2019GL083301>
- Swisdak M, Drake JF (2007) Orientation of the reconnection X-line. *Geophys Res Lett* 34:L11106. <https://doi.org/10.1029/2007GL029815>
- Swisdak M, Rogers BN, Drake JF, Shay MA (2003) Diamagnetic suppression of component magnetic reconnection at the magnetopause. *J Geophys Res* 108(A5):1218. <https://doi.org/10.1029/2002JA009726>
- Toledo-Redondo S, Andre M, Aunai N, Chappell CR, Dargent J, Fuselier SA et al (2021a) Impacts of ionospheric ions on magnetic reconnection and Earth's magnetosphere dynamics. *Rev Geophys* 59:e2020RG000707. <https://doi.org/10.1029/2020RG000707>
- Toledo-Redondo S, Hwang K-J, Escoubet CP, Lavraud B, Fornieles J, Aunai N et al (2021) Solar wind—magnetosphere coupling during radial interplanetary magnetic field conditions: simultaneous multi-point observations. *J Geophys Res Space Phys* 126:e2021JA029506. <https://doi.org/10.1029/2021JA029506>
- Toledo-Redondo S, Hwang K-J, Escoubet CP, Lavraud B, Fornieles J, Aunai N et al (2021b) Solar wind—magnetosphere coupling during radial interplanetary magnetic field conditions: simultaneous multi-point observations. *J Geophys Res* 126:e2021JA029506. <https://doi.org/10.1029/2021JA029506>
- Torbert RB, Burch JL, Phan TD, Hesse M, Argall MR, Shuster JK, Ergun RE, Alm L, Nakamura R et al (2018) Electron-scale dynamics of the diffusion region during symmetric magnetic reconnection in space. *Science* 362:1391–1395. <https://doi.org/10.1126/science.aat2998>
- Trattner KH, Coates AJ, Fazakerley AN, Johnstone AD, Balsiger H, Burch JL, Fuselier SA, Peterson WK, Rosenbauer H, Shelley EG (1998) Overlapping ion populations in the cusp: polar/TIMAS results. *Geophys Res Lett* 25:1621–1624
- Trattner KJ, Fuselier SA, Petrinc SM, Yeoman TK, Moukic C, Kucharek H, Reme H (2005) Reconnection sites of spatial cusp structures. *J Geophys Res* 110:A04207. <https://doi.org/10.1029/2004JA010722>
- Trattner KJ, Mulcock JS, Petrinc SM, Fuselier SA (2007) Probing the boundary between anti-parallel and component reconnection during southwards interplanetary magnetic field conditions. *J Geophys Res* 112:A08210. <https://doi.org/10.1029/2007JA012270>
- Trattner KJ, Petrinc SM, Fuselier SA, Omid N, Sibeck DG (2012) Evidence of multiple reconnection lines at the magnetopause from cusp observations. *J Geophys Res* 117:A01213. <https://doi.org/10.1029/2011JA017080>
- Trattner KJ, Burch JL, Ergun R, Fuselier SA, Gomez RG, Lewis WS, Mauk B, Petrinc SM, Pollock CJ, Phan TD, Vines SK, Wilder FD, Young DT (2016) The response time of the magnetopause reconnection location to changes in the solar wind: MMS case study. *Geophys Res Lett* 43. <https://doi.org/10.1002/2016GL068554>
- Trattner KJ, Burch JL, Ergun R, Eriksson S, Fuselier SA, Giles BL, Gomez RG, Grimes EW, Lewis WS, Mauk B, Petrinc SM, Russell CT, Strangeway RJ, Trenchi L, Wilder FD (2017) The MMS dayside magnetic reconnection locations during phase 1 and their relation to the predictions of the maximum magnetic shear model. *J Geophys Res* 122. <https://doi.org/10.1002/2017JA024488>
- Trattner KJ, Burch JL, Cassak PA, Ergun R, Eriksson S, Fuselier SA, Giles BL, Gomez RG, Grimes EW, Petrinc SM, Webster JM, Wilder FD (2018) The transition between anti-parallel and component magnetic reconnection at Earth's dayside magnetopause. *J Geophys Res* 123. <https://doi.org/10.1029/2018JA026081>
- Trattner KJ, Fuselier SA, Petrinc SM, Burch JL, Ergun R, Grimes EW (2021b) Long and active magnetopause reconnection X-lines during changing IMF conditions. *J Geophys Res* 126. <https://doi.org/10.1029/2020JA028926>
- Trattner KJ, Petrinc SM, Fuselier SA (2021a) The location of magnetic reconnection at Earth's magnetopause. *Space Sci Rev* 217(41). <https://doi.org/10.1007/s11214-021-00817-8>
- Tsyganenko NA, Sitnov MI (2007) Magnetospheric configurations from a high-resolution data-based magnetic field model. *J Geophys Res* 112(A6). <https://doi.org/10.1029/2007JA012260>
- Tsyganenko NA, Andreeva VA, Sitnov MI, Stephens GK, Gjerloev JW, Chu X, Troshichev OA (2021) Reconstructing substorms via historical data mining: is it really feasible? *J Geophys Res Space Phys* 126:e2021JA029604. <https://doi.org/10.1029/2021JA029604>

- Vernisse Y et al (2016) Signatures of complex magnetic topologies from multiple reconnection sites induced by Kelvin-Helmholtz instability. *J Geophys Res* 121:9926–9939. <https://doi.org/10.1002/2016JA023051>
- Vines SK, Fuselier SA, Petrinec SM, Trattner KJ, Allen RC (2017) Occurrence frequency and location of magnetic islands at the dayside magnetopause. *J Geophys Res* 122:4138–4155. <https://doi.org/10.1002/2016JA023524>
- Walsh BM, Komar CM, Pfau-Kempf Y (2017) Spacecraft measurements constraining the spatial extent of a magnetopause reconnection x line. *Geophys Res Lett* 44(7):3038–3046. <https://doi.org/10.1002/2017gl073379>
- Wang X, Chen Y, Tóth G (2022) Simulation of magnetospheric sawtooth oscillations: the role of kinetic reconnection in the magnetotail. *Geophys Res Lett* 49:e2022GL099638. <https://doi.org/10.1029/2022GL099638>
- Webster JM, Burch JL, Reiff PH, Daou AG, Genestreti KJ, Graham DB et al (2018) Magnetospheric multi-scale dayside reconnection electron diffusion region events. *J Geophys Res* 123:4858–4878. <https://doi.org/10.1029/2018JA025245>
- Welling DT, André M, Dandouras I, Delcourt D, Fazakerley A, Fontaine D, Foster J et al (2015) The Earth: plasma sources, losses, and transport processes. *Space Sci Rev* 192(14):145–208. <https://doi.org/10.1007/s11214-015-0187-2>
- Wing S, Johnson JR, Chaston CC et al (2014) Review of solar wind entry into and transport within the plasma sheet. *Space Sci Rev* 184:33–86. <https://doi.org/10.1007/s11214-014-0108-9>
- Wolf RA, Wan Y, Xing X, Zhang J-C, Sazykin S (2009) Entropy and plasma sheet transport. *J Geophys Res* 114. <https://doi.org/10.1029/2009JA014044>
- Wolf RA, Chen CX, Toffoletto FR (2012) Thin filament simulations for Earth's plasma sheet: Interchange oscillations. *J Geophys Res* 117. <https://doi.org/10.1029/2011JA016971>
- Yushkov EV, Petrukovich AA, Artemyev AV, Nakamura R (2021) Thermodynamics of the magnetotail current sheet thinning. *J Geophys Res* 126:e2020JA028969. <https://doi.org/10.1029/2020JA028969>
- Zakharov L, Rogers B, Migliuolo S (1993) The theory of the early nonlinear stage of $m = 1$ reconnection in tokamaks*. *Phys Fluids B* 5:2498. <https://doi.org/10.1063/1.860735>
- Zou Y, Walsh BM, Nishimura Y, Angelopoulos V, Ruohoniemi JM, McWilliams KA, Nishitani N (2019) Local time extent of magnetopause reconnection using space-ground coordination. *Ann Geophys* 37:215–234. <https://doi.org/10.5194/angeo-37-215>
- Zou Y, Walsh BM, Atz E, Liang H, Ma Q, Angelopoulos V (2020) Azimuthal variation of magnetopause reconnection at scales below an Earth radius. *Geophys Res Lett* 47:e2019GL086500. <https://doi.org/10.1029/2019GL086500>
- Zwickl RD, Baker DN, Bame SJ, Feldman WC, Gosling JT, Hones EW Jr, McComas DJ, Tsurutani BT, Slavin JA (1984) Evolution of the Earth's distant magnetotail: ISEE 3 electron plasma results. *J Geophys Res* 89:11007–11012. <https://doi.org/10.1029/JA089iA12p11007>

Publisher's Note Springer Nature remains neutral with regard to jurisdictional claims in published maps and institutional affiliations.

Authors and Affiliations

S.A. Fuselier^{1,2}  · S.M. Petrinec³ · P.H. Reiff⁴ · J. Birn⁵ · D.N. Baker⁶ · I.J. Cohen⁷ · R. Nakamura⁸ · M.I. Sitnov⁷ · G.K. Stephens⁷ · J. Hwang¹ · B. Lavraud⁹ · T.E. Moore¹⁰ · K.J. Trattner⁶ · B.L. Giles¹⁰ · D.J. Gershman¹⁰ · S. Toledo-Redondo¹¹ · J.P. Eastwood¹²

✉ S. Toledo-Redondo
sergio.toledo@um.es

¹ Southwest Research Institute, San Antonio, TX, USA

² University of Texas at San Antonio, San Antonio, TX, USA

³ Lockheed Martin Advanced Technology Center, Palo Alto, CA, USA

⁴ Rice University, Houston, TX, USA

- 5 Space Science Institute, Boulder, CO, USA
- 6 University of Colorado, LASP, Boulder, CO, USA
- 7 Applied Physics Laboratory, Johns Hopkins University, Laurel, MD, USA
- 8 Space Research Institute, Austrian Academy of Sciences, Graz, Austria
- 9 Institut de Recherche en Astrophysique et Planétologie, Université de Toulouse, CNRS, UPS, CNES, Toulouse, France
- 10 NASA, Goddard Space Flight Center, Greenbelt, MD, USA
- 11 Department of Electromagnetism and Electronics, University of Murcia, Murcia, Spain
- 12 Department of Physics, Imperial College London, London, UK